Please cite this article in press as: Sato et al., Spinocerebellar Ataxia Type 31 Is Associated with "Inserted" Penta-Nucleotide Repeats Containing $(TGGAA)_n$..., The American Journal of Human Genetics (2009), doi:10.1016/j.ajhg.2009.09.019

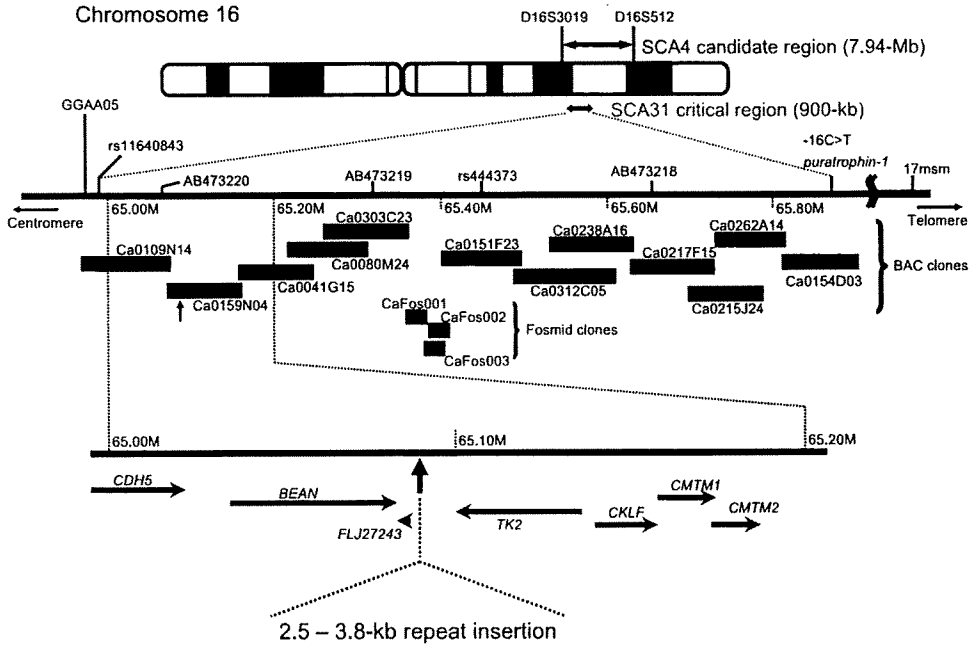

Figure 1. A Comprehensive Physical Map of the 900 kb SCA31 Critical Interval between rs11640843 and −16C > T in the *PLEKHG4* Gene

This region was entirely covered without gaps by 12 BAC and three fosmid clones derived from a SCA31 homozygous patient. These clones were sequenced. An insertion ranging in length from 2.5–3.8 kb was found at nucleotide number 65,081,803 on human chromosome 16 on NCBI build 36.3 between *BEAN* and *TK2*.

performing PCR-based direct sequencing of all coding exons and exon-intron boundaries of *BEAN*, *TK2*, and *FLJ27243* by using 40 primer pairs (shown upon request). Southern blot analysis in the genomic region encompassing *BEAN* and *TK2* (positions from 65,160,201–65,932,756 on chromosome 16, NCBI build 36.3) was also performed similarly to the SCA31 mutation search.

The 21 disease controls[13] who did not have the SCA31 founder haplotypes were also tested for the insertion. Ten out of these 21 individuals were additionally screened for any mutations in *BEAN*, *TK2*, or in *FLJ27243* with the same 40 primer pairs as those used for SCA4.

Results

Southern Blot Analysis Revealed a 2.5–3.8 Insertion Consisting of Complex Pentanucleotide Repeats Containing $(TGGAA)_n$ in SCA31 Patients

Figure 1 shows a comprehensive physical map of the SCA31 critical region. Screening of this 900 kb critical region by Southern blotting allowed us to identify an insertion at nucleotide number 65,081,803 on human chromosome 16 on NCBI build 36.3 (Figures 2A and 2B). There were no other gene rearrangements in the entire critical region. The insertion was found in all 160 affected individuals from 98 SCA31 families, including the individual in the U9 family previously described,[13] and ranged in length from 2.5–3.8 kb. PCR amplification followed by direct sequencing or shotgun sequencing of the insert disclosed that the insertion consisted of a preceding four nucleotides, "TCAC," and the three penta-nucleotide repeat components $(TGGAA)_n$, $(TAGAA)_n$, and $(TAAAA)_n$ in all SCA31 patients tested (Figure 2C). In the homozygous patient's repeat, which was sequenced by the shotgun method, a pure $(TGGAA)_n$ stretch extended for at least 110 repeats, presumably for more than 1 kb in light of the size of the sheared DNA fragment. Pure $(TAAAATA\ GAA)_n$ also stretched for more than 112 repeats. These pure repeat sequences were separated by a bridging sequence and $(TAGAA)_{46}$.

In contrast to SCA31 chromosomes, the vast majority of controls (99.77% among 800 Japanese and 60 white American chromosomes) did not have any insertions. The 21 disease controls and SCA4 subjects also did not have this insertion. Very rarely, however, insertions were observed in two individuals (2/860 chromosomes: 0.23%) (controls 1 and 2) (Figure 2A, left-hand panel). PCR amplification and sequencing showed that the inserts were in the same position as in the SCA31 patients, and their lengths were 1.5 kb in control 1 and 2.0 kb in control 2. Sequencing analysis of controls 1 and 2 disclosed that they both had inserts with a preceding 4 base "TCAC," $(TAAAA)_n$, $(TAGAA)_n$, and $(TAAAATAGAA)_n$ stretch (Figure 2D). However, no (TGGAA) sequences were observed. Because these individuals did not manifest any cerebellar signs or have any documented histories of inherited diseases in their families, we considered that these inserts with complex penta-nucleotide repeats were not pathogenic, or at least did not have enough toxicity to develop a disease during

Please cite this article in press as: Sato et al., Spinocerebellar Ataxia Type 31 Is Associated with "Inserted" Penta-Nucleotide Repeats Containing (TGGAA)n..., The American Journal of Human Genetics (2009), doi:10.1016/j.ajhg.2009.09.019

the human lifespan. Therefore, we concluded that the insertions in SCA31 patients exerted their toxicity either because of their lengths (> = 2.5-kb) or because of their $(TGGAA)_n$ component, which made a clear distinction between SCA31 and the rare control insertions.

The insertion site was identical for all insertions, and the junction point of the insertion was located at the 3′-tail of an AluSx[25] (Figure 2B). Alu variants have previously been linked to certain disease loci, such as DM1, HD, Friedreich ataxia (FRDA) (MIM #229300), and fragile X syndrome (FRAXA) (MIM #300624).[26] There is a related short penta-nucleotide repeat of $(TAAAA)_n$ immediately downstream of the insertion site (Figure 2B). This $(TAAAA)_n$ was polymorphic ("n" usually ranged from 8–21), and a very rare expansion up to approximately 140 repeats was observed in one out of 860 control chromosomes (frequency: 0.12%) (control 1, shorter allele; see Figure 2A, left-hand panel). Both $(TAAAA)_n$ and the SCA31 founder insertion are polypurine tracts interrupted with thymidines. SCA31 is similar to Friedreich's ataxia (FRDA) in that they both contain "GAA."

The Length of the SCA31 Insertion Is Inversely Correlated with the Age of Onset

The SCA31 penta-nucleotide repeat insertion ranged from 2.5–3.8 kb in length (Figure 3A). Although SCA31 is a disease with a strong founder effect, the fact that the length of the insertion varied by ~1.3 kb among families suggests that the insertion was not completely stable during multiple transmissions from one or a few principal ancestors. Importantly, a significant correlation was observed in that patients with longer repeats show earlier disease onset ($r = -0.41$, $p = 0.010$, $n = 39$) (Figure 3B). Very mild anticipation (younger age of onset in future generations) is sometimes observed in SCA31[8], which suggests that the insertion might have a propensity for expansion. Indeed, we detected a subtle expansion of the inserted repeat within one SCA31 family (Figure 3C).

Complete Genomic Sequencing of the 900 kb Critical Region Unveiled Only Two Mutation Candidates

Because of the strong founder effect in SCA31, we needed to detect all genetic changes in the critical region. For this reason, we also performed BAC- and fosmid-based shotgun sequencing over the entire 900 kb SCA31 critical region. Upon completing entire sequencing in the homozygous patient, we initially found 336 sites annotated differently from the reference sequence (NCBI build 36.3). However, most of these 336 changes were also found in the controls, allowing us to exclude them as mutation candidates. In the course of this effort, we also investigated 34 new SCA31 patients and found that two independent SCA31 patients shared the disease-specific haplotype only between AB473214 and AB473219 (Table 2). As a result, we finally found that the penta-nucleotide repeat insertion and a single-nucleotide change (AB473217) at 65,114,245 are the only genetic changes segregating with the disease. This single-nucleotide change (AB473217) is in an intron of the *TK2* (thymidine kinase 2) gene, 4,964 nucleotides distant from the nearest splice junction. RT-PCR analysis did not indicate the presence of aberrant transcripts in SCA31 patients (data shown upon request). Quantitative genomic PCR and aCGH did not show copy-number variations in the SCA31 critical region (data shown upon request). Taking all these data together, we considered that the complex penta-nucleotide repeat insertion containing $(TGGAA)_n$ was the only mutation that could plausibly cause SCA31. Further efforts were focused on this repeat insertion.

The SCA31 Repeat Insertion Is Located in Newly Indentified Introns of BEAN and TK2

According to the NCBI database (build 36.3), the insertion was located between two genes, *BEAN* and *TK2*, and also upstream of an EST, *FLJ27243* (Figure 1). However, we found previously unidentified downstream exons for *BEAN* and *TK2*, demonstrating that the insertion is in introns of these two genes transcribed in opposite directions (Figure 4). We confirmed by RT-PCR that the extended versions of *BEAN* and *TK2*, which we named *BEAN-EXT* and *TK2-EXT*, respectively, and *FLJ27243* are all expressed at low levels in the brain (Figures 5A–5C). Notably, *BEAN-EXT*, as well as *BEAN*, is expressed exclusively in the brain. However, neither ordinary nor quantitative RT-PCR proved that the repeat insertion caused splicing abnormalities or alterations in the expression levels of *BEAN*, *TK2*, or other nearby genes (Figure 5D).

The Transcribed SCA31 Insertion Forms Nuclear Foci in Purkinje Cells

We next performed in situ hybridization to see whether transcribed repeat sequences form aggregates ("RNA foci") in nuclei, as in RNA-mediated noncoding repeat-expansion disorders,[3] such as DM1[23] and DM2.[27] Using an LNA probe targeting $(UAAAAUAGAA)_n$, we detected RNA foci in approximately 30%–50% of the nuclei of SCA31 patients' Purkinje cells (Figure 6). Such RNA foci were never observed in controls, allowing a clear distinction. This might indicate not only that the insertion is transcribed as *BEAN-EXT* transcript in SCA31 brains but also that the insertion transcribed in the direction of *BEAN-EXT* forms abnormal RNA aggregates in Purkinje cells, the primary target of SCA31. Foci were never observed with a probe for anti-sense $(UUCUAUUUUA)_n$ repeats corresponding to the *TK2-EXT* transcripts in either SCA31 or control brains.

$(UGGAA)_n$, the Disease-Specific Transcribed Component of the SCA31 Insertion, binds to SFRS1 and SFRS9 In Vitro

We next searched for proteins that could potentially bind to the transcribed SCA31 insertion, particularly to the $(UG\ GAA)_n$ sequence. Accumulating evidence increasingly suggests that satellite III (SatIII), the paracentromeric

Please cite this article in press as: Sato et al., Spinocerebellar Ataxia Type 31 Is Associated with "Inserted" Penta-Nucleotide Repeats Containing $(TGGAA)_n$..., The American Journal of Human Genetics (2009), doi:10.1016/j.ajhg.2009.09.019

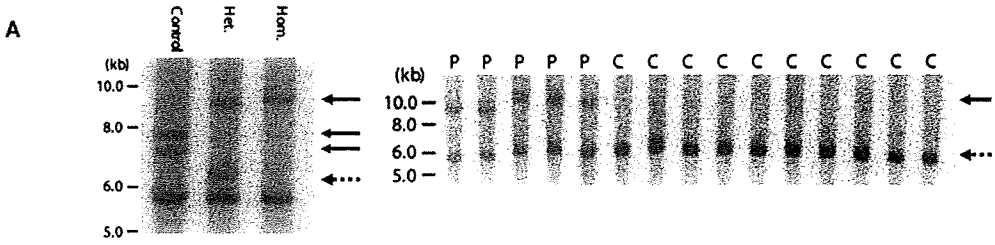

B

ACTCCAACTGGGATGCAGTTTCTCAATCAAAGGGATATGAACTGCCCTGGCCACTGAATTCAGAGAACATTGTAGGGGGCAGGGGAGTTGGGAGCAGG
GAGCAGAGATCCCAGCTGTGACGAGCCCAGGTCTGAGGCAGCTCCAAGACCAAGCACCCAGGTGGCTGTCCTTCCTGGCGACTGGAGAGGCAGGAGC
CCAGCAGAGTCTCATAGAAAGCAAATGACAATCAAGACCCAGGTCCTCAGCCAGATGCGGTGGCTCATGCCTGTAATCTCAGCACTTTGGGAGGCCAAA
GTGGGCAGATCACCTCAGGTCAGGAGTTTGAGATCAGCCTGGCCAACATGGTGAAATCCCATCTCTACTAAAAAAAAAAAAAAAAAAAAAAAAAAATTA
GCCAGGCATAGTGGCACATGCATGTAGTCCCAACTACTTGGGAGGCTGAGGCAGGAGAATCGCTTGAACCCAGAAGGTGGAAATTGCAGTGGGCCAAG
ATCACGTCACTGCACTCCAGCCTGGGCAACAAAACAAGACTCTGTTTCAA-(insertion)-TAAAATAAAATAAAATAAAATAAAATAAAATAAAATAAA
ATAAAATAAAATAATAAAATAAAAAGAAACCTCTAAATTGATTGAGATCTGCCTCCGACACTTTTCAATTTACAAAAACATACCTAAGAATTGGCCACCCAG
GGGCAGGAAGCTGGGGTTTCTATCCAGTAACTCTCACCCCGCTGGCCCTTGGTTGGTTGAGGGTCGCCACCTTCCTGGCGCTTCCAGCCTGTCCCGCA
CACTAGCAGAGTATGCCTCTGCAGCCAGCAGCACTCAAGGCATGAGGCATTACTGGGGATATCTGGATGGGATGGTAGTGTGGAAAGATGCAGATGCT
GATGTGCCTGGTCTTCATTTTTTGTGGGGCAGGGGGACAAAGAAAGGACAAATCCTGACCTAGGCCCTGCTCCACTGGGAGGGGCCCGGTCACCCTCC
AATCTCAGCTTTTCAGAGTGACAAGCAGTGGCAGGGCCTGGCTGCACATAGCTTTATCTCTTGCTAGCACAACTTCCTCCTTTGCTTCCAGATTGGGCTT
TGGAGCAGGAGAGGCAGGACCCATCCATTCCTCCAAGTGCCCAGCCTGAGCCTGGCCTGGGACAGGACTCTATCCTCCATATCCAGCCCCCCCGAAGC
CACCATGAGCAGGTCCCAATCCCCAGGCCCAGGCGAAGCTGCTCTGGGTGAGACCCTCCTGGGCAACATCATCAGCTACTACCAGGAGAGAGCAGGG
GAGGGCCGGCTCGATGTCTGCAGGCAAGCAGCCCTCACCCACAGGGCCAGGTGGCTCCTGGGCAGGAGGGCCCCTCCATGGCTCTGTCTGCCAGAG
GAAGTGGCCCTTGCTCTGGGTGGCTGCTGTTGTGGGGATCCCAGCCCTGTCCCAAAAGTCAGCCCTGAGCTGGTGCATGCACTAGAGTTCCTGGAGCT
GATCTCTGTCAACCTGCTTCTGTTTCCCTGGAGGAAGGAAATCAGGTCCCTAAAG

C

SCA31 insertion sequence:

[TCAC TAAAA (TAGAA)2 (TGGAA)n TGGGAA TGGAA TGGGAA (TAGAA)2 (TGGAA)2 (TAGAA)2 TGGAA (TAGAA)46 (TAAAA TAGAA)n]

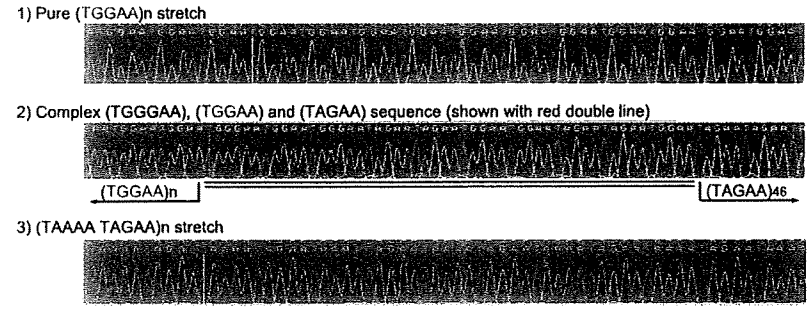

D [TCAC (TAAAA)2 AAA (TAAAA)3-5 AA (TAAAA)2 TA TAAAA TAGAA TAAAA (TAGAA)n(TAAAATAGAA)n]

(allele frequency: 0.23% in control)

Figure 2. Identification of Complex Pentanucleotide Repeat Insertions in SCA31 Patients

(A) Southern blot analysis showing the SCA31 insertion. The left-hand panel shows EcoRI-digested genomic fragments detected with a cosmid probe for the region between nucleotides 65,083,571 and 65,124,051. A rare 1.5 kb insertion and an unusual 0.7 kb expanded $(TAAAA)_n$ (both shown with solid black arrows) were observed in one control (control 1). SCA31 insertions in two patients are shown with a red arrow. "Hom." and "Het." designate the homozygous patient and heterozygous patient, respectively. The dotted arrow indicates normal chromosomes without insertions. The thick 5.8 kb bands common in the three subjects show fragments outside the insertion site. The right-hand panel shows aberrant EcoRI-digested 9–10 kb genomic fragments (a red arrow) that completely segregated with SCA31 patients (P). All heterozygous patients (P) and controls (C) have "normal" 6 kb fragments (dotted arrows). Radiolabeled PCR products obtained by amplifying the 3009 bp genomic segment between nucleotides 65,079,127 and 65,082,135 on NCBI build 36.3 were used as probes.

(B) Sequences around the SCA31 insertion (chromosome16: nucleotides 65,081,260–65,082,786 on NCBI build 36.3). Flanking primers for PCR amplification (underlined in red) of insertion and flanking HaeIII recognition sites (in shaded boxes) are shown. The *AluSx* sequence[30] is shown with a green underline. Without an insertion, PCR amplification with flanking primers and a subsequent HaeIII digestion will produce a DNA fragment 193 bp in length.

Please cite this article in press as: Sato et al., Spinocerebellar Ataxia Type 31 Is Associated with "Inserted" Penta-Nucleotide Repeats Containing $(TGGAA)_n$..., The American Journal of Human Genetics (2009), doi:10.1016/j.ajhg.2009.09.019

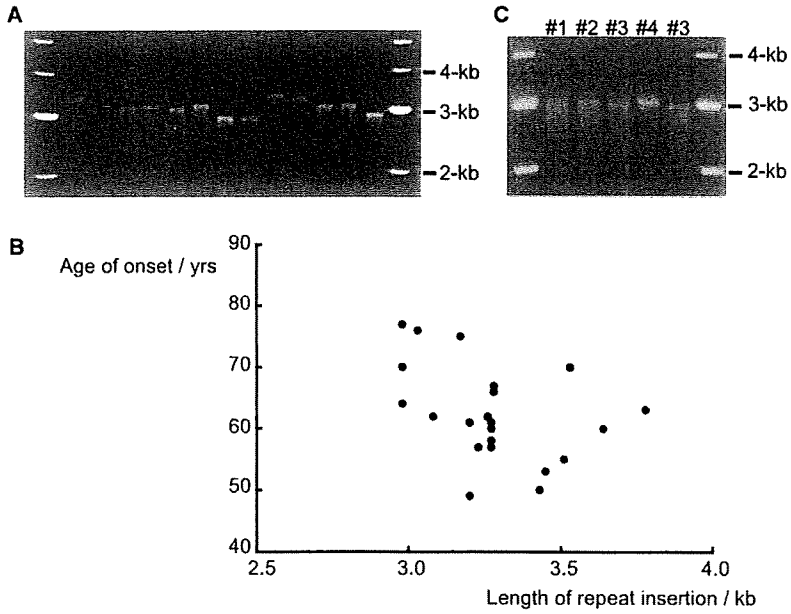

Figure 3. The Length of Insertion Inversely Correlates with Age of Onset in SCA31

(A) PCR amplification and agarose gel electrophoresis showing that the length of the insertion differs among SCA31 families.

(B) A scatter plot showing an inverse correlation between the length of the SCA31 insertion and the age of onset. The length of the repeat insertion was inversely correlated with age of onset (Pearson's product-moment correlation coefficient $r = -0.41$, $p = 0.010$, $n = 39$.).

(C) A slight expansion of the SCA31 insertion observed in one SCA31 family. Individual #4 has a slightly longer insertion than the others (#1–#3) in the same SCA31 family. This individual #4 is in the youngest generation among them.

repetitive sequences rich in $(TGGAA)_n$, are transcribed under stress[28–30] to form nuclear stress bodies (nSBs) and play an important role in regulating the splicing machinery by recruiting certain splicing factors,[31] such as serine/arginine-rich splicing factor (SFRS) 1 (also known as ASF/SF2 or SRp30a) and SFRS9 (SRp30c), to nSBs. Onthe basis of this fact, we performed EMSAs and found that SFRS1 and SFRS9 directly bind to $(UGGAA)_n$, the transcribed sequence of $(TGGAA)_n$, in vitro (Figure 7).

$(TGGAA)_n$ Is Abundant in Heterochromatin, Particularly in Centromeric Regions

In order to see the distribution of $(TGGAA)_n$ in the human genome, we also performed an in silico search for $(TGGAA)_n$ and found that these penta-nucleotide repeats are indeed abundant in the centromeres of chromosomes 2, 4, 7, 10, 16, 17, 20, and Y (Figure 8A). On the other hand, $(TAGAA)_n$ is observed in euchromatins and telomeres (Figure 8B). $(TAAAATAGAA)_n$ was not detected in the human genome.

SCA4 and SCA31 Are Not Likely to Be Allelic

Neither the SCA31 insertion nor the single-nucleotide change in *TK2* (AB473217) was detected in SCA4 individuals. PCR-based direct sequencing of all coding exons and exon-intron boundaries of *BEAN*, *TK2*, and *FLJ27243* with 40 primer pairs and Southern blot analysis in the genomic region encompassing *BEAN* and *TK2* were also negative. These results did not support the hypothesis that SCA4 and SCA31 were allelic diseases. Similarly, the 21 disease controls[13] also did not harbor the insertion. Mutations in *BEAN*, *TK2*, and *FLJ27243* were not found in the ten disease controls tested.

Discussion

In summary with regard to the results of our mutation search, only two genetic changes were found to completely segregate with the disease: the complex penta-nucleotide repeat insertion at nucleotide 65,081,803 and a single-nucleotide change (AB473217) at nucleotide 65,114,245 in human chromosome 16 (NCBI build 36.3). The single-nucleotide change, located in an intron, did not seem to have any obvious effects on splicing or expression patterns, providing no evidence that this is the causative mutation. On the other hand, the length of the insertion with penta-nucleotide repeats was inversely correlated with age of onset, in agreement with the general rules of repeat-expansion disorders.[1–3] We therefore concluded that the penta-nucleotide repeat insertion containing $(TGGAA)_n$ is the only likely candidate for the SCA31 mutation. The fact that we did not find any allelic mutations in *BEAN*, *TK2*, or *FLJ27243* in our cohort of patients (5 SCA4 and 21 disease-control individuals) does not deny this conclusion because none of the repeat-expansion diseases, except SCA6, have allelic mutations.[1–3]

All the previously known repeat-expansion disorders are caused by expansions of microsatellites present as polymorphic DNA repeats in humans: normal individuals

(C) The components of the SCA31 insertion in the homozygous patient. The SCA31 insertion consists of a preceding 4 bp TCAC and three different penta-nucleotides, $(TGGAA)_n$, $(TAGAA)_n$, and $(TAAAA)_n$. $(TGGAA)_n$ is the patient-specific repeat (shown in red), and both $(TGGAA)_n$ and $(TAAAATAGAA)_n$ are pure stretches too long to be read through. The bridging sequence between $(TGGAA)_n$ and $(TAGAA)_{46}$ is underlined in red.

(D) The sequence of the insertion in control 1. Rare insertions were observed in controls at the same position as the SCA31 insertion, but with shorter length and different components. The insertion in control 1 consisted of a preceding 4 bp TCAC and two pentanucleotide components, $(TAGAA)_n$ and $(TAAAA)_n$. The $(TGGAA)_n$ was not detected.

Please cite this article in press as: Sato et al., Spinocerebellar Ataxia Type 31 Is Associated with "Inserted" Penta-Nucleotide Repeats Containing $(TGGAA)_n$..., The American Journal of Human Genetics (2009), doi:10.1016/j.ajhg.2009.09.019

Table 2. The Haplotypes of Representative SCA31 Patients and Control Subjects

Polymorphic markers Site on NCBI Build 36.3		rs11640843 64,982,677	AB473214* 65,024,796	AB473220 65,049,291	Complex penta-nucleotide repeat insertion* 65,081,803	AB473217* 65,114,245	AB473219 65,337,827	AB473218* 65,658,263	-16C>T *puratrophin-1* 65,871,433
Reference sequence (NCBI Build 36.3)		**C**	**G**	**G**	-	**G**	**A**	**T**	**C**
Frequencies in controls		C 72.2 % T 27.8 %	G 99.0 % A 1.0 %	G 99.2 % A 0.8 %	(See Fig.2B, C and D.)	G 100.0 % C 0.0 %	A 100.0 % G 0.0 %	T 100.0 % C 0.0 %	C 100.0 % T 0.0 %
Patients	Homozygous patient	T	A	A	TCAC- (TGGAA)n (TAGAA)n (TAAAA TAGAA)n	C	G	C	T
	P4	T	G	A	TCAC- (TGGAA)n (TAGAA)n (TAAAA TAGAA)n	C	G	C	T
	T46	C	G	A	TCAC- (TGGAA)n (TAGAA)n (TAAAA TAGAA)n	C	G	C	T
	T47*	C	G	G/A	TCAC- (TGGAA)n (TAGAA)n (TAAAA TAGAA)n	C/G	A	T	C
	T48*	C	G	G/A	TCAC- (TGGAA)n (TAGAA)n (TAAAA TAGAA)n	C/G	A	T	C
Controls	Control 1	T	G/A	G/A	TCAC- (TAGAA)n (TAAAA TAGAA)n	G	A	T	C
	Control 2	C/T	G	G	TCAC- (TAGAA)n (TAAAA TAGAA)n	G	A	T	C

The founder haplotype is shown with a yellow background. New markers and families analyzed in this study are marked with an asterisk (*). Although the single nucleotide change (AB473220) was seen in all SCA31 patients, it was also seen in control 1, excluding it as a mutation candidate. The two genetic changes segregating with SCA31 are shown in the red box.

have smaller numbers of repeats, whereas patients harbor longer repeats.[26] To our knowledge, SCA31 is the first human disease discovered to be associated with a microsatellite "insertion." The observation in rare controls of shorter inserted repeats lacking $(TGGAA)_n$ suggests that the inserted microsatellite has to have sufficient length ($\geq$ 2.5 kb), the $(TGGAA)_n$ stretch, or both to cause the disease. Notably, haplotypes based on flanking markers were not similar in the controls with the rare inserts and the SCA31 patients. Although this might indicate that the insertions in controls and SCA31 patients arose from different insertion events, concluding so is still premature. Both the control and SCA31 inserts had a preceding 4 bp TCAC and also possessed $(TAGAA)_n$, $(TAAAA)_n$, and $(TAAAATAGAA)_n$. In fact, controls with rare premutation alleles in the DM2 repeat were found to have a haplotype similar to that of DM2 patients.[32] Thus, further analysis will need to address whether SCA31 and control insertions have different ancestries.

The presence of $(TGGAA)_n$, the characteristic sequence of satellites II and III[33], suggests that the SCA31 insertion might be related to heterochromatin; this idea is supported

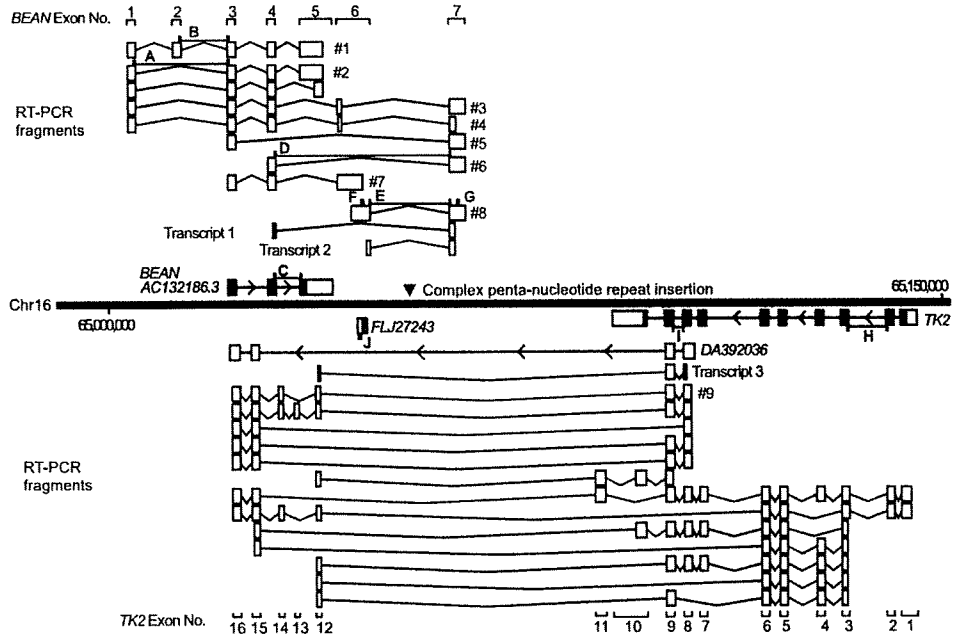

Figure 4. Various Transcripts Spanning the SCA31 Repeat Insertion Site
The locations of *BEAN*, *TK2*, *FLJ27243*, and the SCA31 insertion (red arrowhead) are shown on the physical map of the chromosomal region between nucleotides 65,000,000 and 65,150,000 on NCBI build 36.3. Exons registered in the NCBI database are shown with black boxes, and 5′- and 3′-UTRs are shown with white boxes attached to them. Although the SCA31 insertion is located in the intergene region between *BEAN* and *TK2* on the NCBI database, various newly identified transcripts of these genes (shown with white boxes with their exon numbers) were detected by RT-PCR, and some of them encompassed the SCA31 insertion. The insertion appeared to be located in introns of *BEAN* and *TK2*, two genes transcribed in opposite directions. DA392036 annotated in the NCBI database seemed to be a part of *TK2-EXT*. Transcripts 1–3 correspond to the transcripts detected by RT-PCR in Figures 5A and 5B (Table S1). The primer pairs for RT-PCR are shown with small blue boxes (A–J; Figure 5D and Tables S1 and S2).

Please cite this article in press as: Sato et al., Spinocerebellar Ataxia Type 31 Is Associated with "Inserted" Penta-Nucleotide Repeats Containing $(TGGAA)_n$..., The American Journal of Human Genetics (2009), doi:10.1016/j.ajhg.2009.09.019

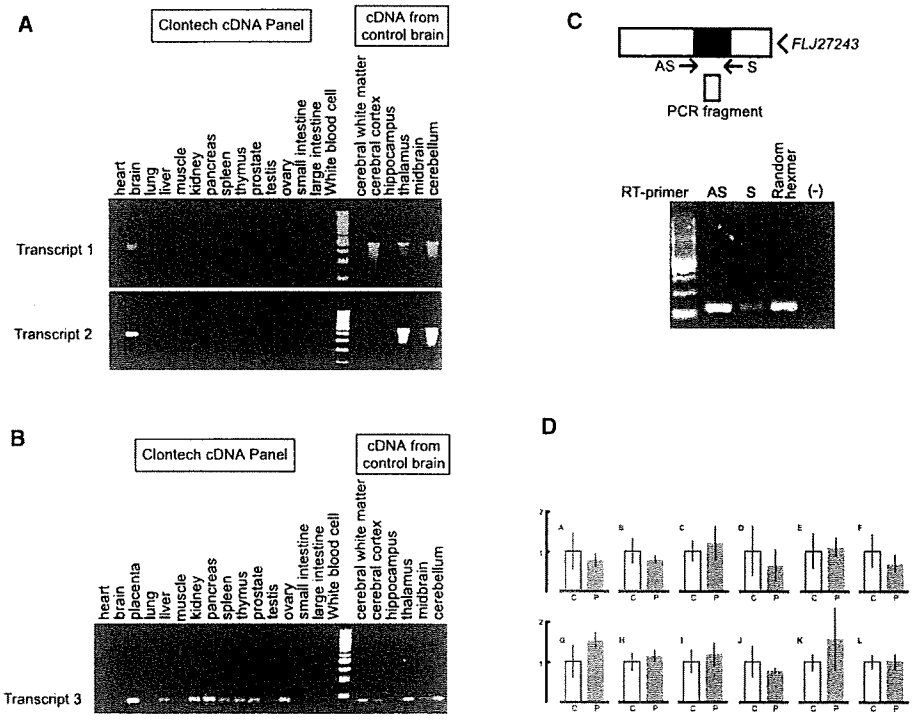

Figure 5. Gene Expression of *BEAN-EXT*, *TK2-EXT*, and *FLJ27243* in Humans
(A) RT-PCR analysis for *BEAN-EXT* mRNA (transcripts 1 and 2 in Figure 5) showing its brain-specific expression.
(B) RT-PCR analysis for *TK2-EXT* mRNA (transcript 3 in Figure 5) showing higher expression in various systemic organs than in the brain.
(C) RT-PCR of *FLJ27243* mRNA in the human cerebellum. Strand-specific RT-PCR shows expression of *FLJ27243*, represented by "RT with AS primer," in the brain. The "S primer" represents transcription in the orientation of *BEAN*, and "Random Hexamer" indicates transcripts in both directions. The specificity of this strand-specific RT-PCR is confirmed by negative amplification when reverse transcriptase is omitted [(-)].
(D) Quantitative RT-PCR on *BEAN*, *TK2*, *FLJ27243*, and *CKLF* mRNAs in controls' (n = 4) and patients' (n = 2) cerebella. The locations of RT-PCR primer and probe sets (A–J) are indicated in Figure 5 (C: controls; P: patients; the scale bar represents 1 SD) (see Table S2 for probe sequences). No consistent difference was found in the expression levels of *BEAN* (including *BEAN-EXT*; probe sets: A–G), *TK2* (probe sets H and I), *FLJ27243* (probe set J), or *CKLF* (probe sets K–L) mRNAs compared in the control versus SCA31 patient groups.

by our in silico search for $(TGGAA)_n$. SCA31 could be the second disease associated with heterochromatin insertion after autosomal-recessive congenital deafness (DFNB10) (MIM #605316),[34] caused by a β-satellite sequence insertion into a coding exon. Although the β-satellite sequence insertion causes DFNB10 via a loss-of-function mechanism, SCA31 appears to be associated with intronic repeat insertions that are transcribed to form RNA foci.

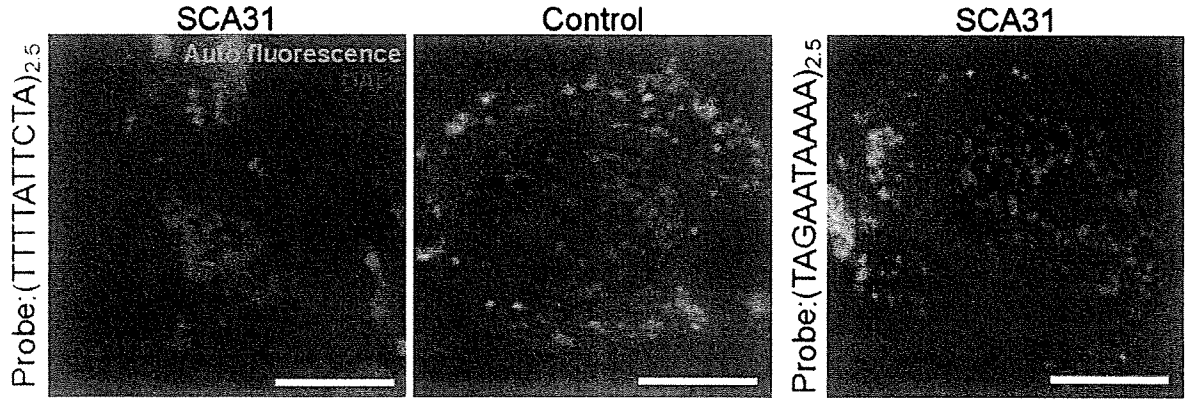

Figure 6. Presence of RNA Foci in SCA31 Purkinje Cells
RNA foci (red dots) seen in a nucleus (stained with DAPI; blue) of an SCA31 Purkinje cell with an LNA-$(TTTTATTCTA)_{2.5}$ probe targeting the transcripts containing the $(UAAAAUAGAA)_n$ repeat (autofluorescence; orange). In controls, foci were completely negative. Antisense transcripts, searched with an LNA-$(TAGAATAAAA)_{2.5}$ probe, did not appear as RNA foci. Scale bars represent 10 μm.

Please cite this article in press as: Sato et al., Spinocerebellar Ataxia Type 31 Is Associated with "Inserted" Penta-Nucleotide Repeats Containing $(TGGAA)_n$..., The American Journal of Human Genetics (2009), doi:10.1016/j.ajhg.2009.09.019

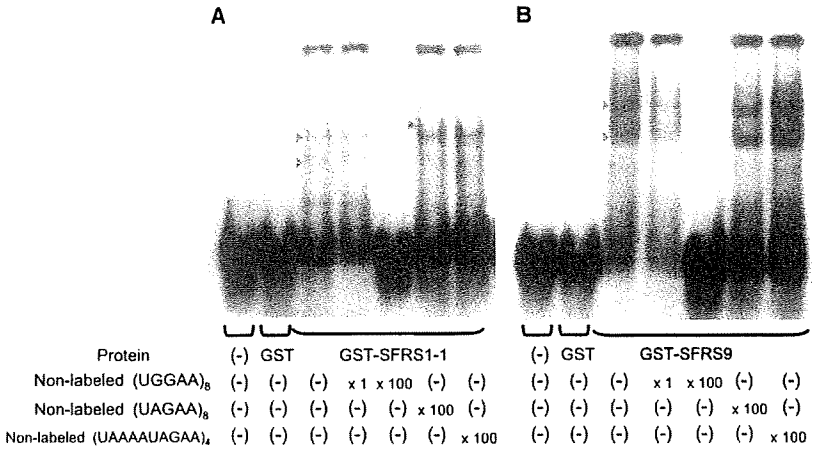

Figure 7. The Pentanucleotide $(TGGAA)_n$ Binds to Splicing Factors SFRS1 and SFRS9 In Vitro

EMSA showing specific binding of SFRS1 isoform 1 (SFRS1-1) (A) and SFRS9 (B) to RNA oligonucleotide $(UGGAA)_8$. Shifted bands (arrowheads) were observed in mixtures of digoxigenin(DIG)-$(UGGAA)_8$ and either GST-SFRS1-1 or GST-SFRS-9. The shifted bands disappeared with the addition of nonlabeled $(UGGAA)_8$, whereas the addition of excess amounts of nonlabeled $(UGGAA)_8$ or $(UAAAAUAGAA)_4$ did not interfere with the band shift. No shift was seen when DIG-$(UGGAA)_8$ was mixed with GST alone.

How does this insertion cause the disease? Haplo-insufficiency or dominant-negative mechanisms do not appear likely because both *BEAN* (including *BEAN-EXT*) and *TK2* (including *TK2-EXT*) were expressed at the same level in SCA31 patients' brains as they were in control brains, at least at mRNA levels. Paracentromeric satellite sequences rich in penta-nucleotide repeats $(TGGAA)_n$ are thought to have various essential roles, such as the maintenance of chromatin conformation.[33] The expanded repeat sequence of $(TGGAA)_n$, which tends to take non-B DNA structures,[33] might induce local chromosomal structural changes that could alter the expressions of other genes, as proposed in FRDA caused by $(GAA)_n$ expansion ("sticky DNA").[1]

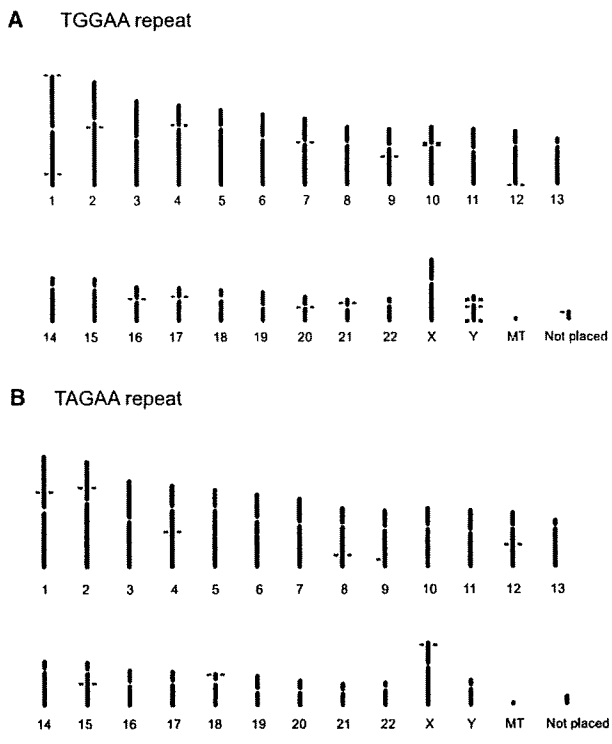

Figure 8. $(TGGAA)_n$ Is Particularly Abundant in Centromeric Regions

(A) $(TGGAA)_{40}$ sequences are abundant in the centromeres of chromosomes 2, 4, 7, 10, 16, 17, 20 and Y, whereas they are sparse in normal euchromosomes.

(B) $(TAGAA)_{40}$ sequences are widely observed in euchromatin as well as in telomeres.

Alternatively, there is a possibility that the transcripts of the repeat insertion convey the pathogenesis (i.e., "RNA-mediated gain-of-function mechanism").[3] Earlier onset in homozygotes than in heterozygotes, as described in a previous study[14], appear to support the gain-of-function mechanism. In noncoding repeat expansion disorders, such as DM1[23], DM2[27], FXTAS[35], HDL2[36], and SCA8[22], transcribed repeats form aggregates ("RNA foci") in the nuclei of affected cells. The sequestration of proteins that bind to these foci, such as muscleblind-like protein 1 and CUG-binding protein (CUG-BP)1[3] in DM1 and DM2, as well as CUG-BP1 and heterogeneous nuclear ribonucleoprotein (hnRNP)A2 in FXTAS[37], are believed to cause dysregulation of alternative splicing. In light of these facts, the presence of nuclear RNA foci in Purkinje cells and in vitro binding of essential splicing factors SFRS1 and SFRS9 to $(UGGAA)_n$ implies that SCA31 might also be associated with RNA-mediated gain-of-function mechanisms.

SR proteins, such as SFRS1, play important roles in constitutive splicing, alternative splicing regulation in which they antagonize hnRNPs[31,38], and stabilizing mRNAs.[38] Suppression of SFRS1 expression results in embryonic lethality in *C. elegans*[39] and death in particular subsets of neurons.[40] If the transcripts of the SCA31 insertion should indeed sequester SFRS1 and SFRS9 by forming RNA foci, it might disturb the pre-mRNA processing patterns of various genes[41] and ultimately lead to neuronal death. Interestingly, overexpression of *hsrω*, the *Drosophila* noncoding RNA gene similar to SatIII, is shown to exacerbate neurodegeneration in a fly model of polyglutamine disease, in which sequestration of transcription factors such as CREB binding protein (CBP) are considered important for pathogenesis.[42] Further analysis is clearly needed,

Please cite this article in press as: Sato et al., Spinocerebellar Ataxia Type 31 Is Associated with "Inserted" Penta-Nucleotide Repeats Containing $(TGGAA)_n$..., The American Journal of Human Genetics (2009), doi:10.1016/j.ajhg.2009.09.019

not only to dissect how this newly indentified insertion mutation causes a human disease, but also to disclose the roles of highly repeated sequences in heterochromatin.

Supplemental Data

Supplemental Data include four tables and can be found with this article online at http://www.cell.com/AJHG.

Acknowledgments

We would like to thank the families who participated in this study, as well as Iku Sudo, Minori Kono, and Hideko Uno for their technical assistance. This study was funded by numerous grants, particularly from the Health and Labour Sciences Research Grants on Human Genome (KI) and Ataxic Diseases (HM), Ministry of Health, Labour and Welfare, Japan, and the 21st Century COE Program, Brain Integration and its Disorders, the Ministry of Education, Science and Culture, Japan (HM). We also thank Laura P.W. Ranum (University of Minnesota) and Christopher E. Pearson (Hospital for Sick Children, Toronto) for their advice. We thank Eric Sheldon (Scientific Language Editing Team, Tsukuba, Japan) for proofreading our manuscript.

Received: May 19, 2009
Revised: August 25, 2009
Accepted: September 21, 2009
Published online: October 29, 2009

Web Resources

The URLs for data presented herein are as follows:

BLAST, http://blast.ncbi.nlm.nih.gov/Blast.cgi
dbSNP, http://www.ncbi.nlm.nih.gov/SNP/
DDBJ, http://www.ddbj.nig.ac.jp/
ESEfinder 3.0, http://rulai.cshl.edu/cgi-bin/tools/ESE3/esefinder.cgi?process=home
Online Mendelian Inheritance in Man (OMIM), http://www.ncbi.nlm.nih.gov/sites/entrez?db=OMIM
NCBI, http://www.ncbi.nlm.nih.gov/

Accession Numbers

The GenBank accession numbers for *Homo sapiens BEAN-EXT* transcripts are AB472390 (#1 in Figure 5), AB472391 (#2), AB472392 (#3), AB47233 (#6), AB472395 (#7), AB472396 (#4), AB472398 (#8), and AB472399 (#5). The GenBank accession number for *Homo sapiens TK2-EXT* transcript is AB472397 (#9 in Figure 5). The GenBank accession number for human genome single nucleotide polymorphisms (SNPs) are AB473214; 65,024,796 G/A: AB473217; 65,114,245 G/C: AB473218; 65,658,263 T/C: AB473219; 65,337,827 A/G: AB473220; and 65,049,292 G/A. For the insertion site at 65,081,803, the accession number is AB473216; for the control insertion, the accession number is AB473734; and for the insertion in the SCA31 patient, the accession number is AB473733.

References

1. Brice, A., and Pulst, S.-M. (2007). Spinocerebellar degenerations: The ataxias and spastic paraplegias (Philadelphia: Butterworth Heinemann, Elsevier, Inc.).
2. Zoghbi, H.Y., and Orr, H.T. (2000). Glutamine repeats and neurodegeneration. Annu. Rev. Neurosci. *23*, 217–247.
3. Ranum, L.P.W., and Cooper, T.A. (2006). RNA-mediated neuromuscular disorders. Annu. Rev. Neurosci. *29*, 259–277.
4. Bandmann, O., and Singleton, A.B. (2008). Yet another spinocerebellar ataxia: The saga continues. Neurology *71*, 542–543.
5. Nagaoka, U., Takashima, M., Ishikawa, K., Yoshizawa, K., Yoshizawa, T., Ishikawa, M., Yamawaki, T., Shoji, S., and Mizusawa, H. (2000). A gene on *SCA4* locus causes dominantly inherited pure cerebellar ataxia. Neurology *54*, 1971–1975.
6. Ishikawa, K., Toru, S., Tsunemi, T., Li, M., Kobayashi, K., Yokota, T., Amino, T., Owada, K., Fujigasaki, H., Sakamoto, M., et al. (2005). An autosomal dominant cerebellar ataxia linked to chromosome 16q22.1 is associated with a single-nucleotide substitution in the 5′ untranslated region of the gene encoding a protein with spectrin repeat and Rho guanine-nucleotide exchange-factor domains. Am. J. Hum. Genet. *77*, 280–296.
7. Flanigan, K., Gardner, K., Alderson, K., Galster, B., Otterud, B., Leppert, M.F., Kaplan, C., and Ptácek, L.J. (1996). Autosomal dominant spinocerebellar ataxia with sensory axonal neuropathy (SCA4): Clinical description and genetic localization to chromosome 16q22.1. Am. J. Hum. Genet. *59*, 392–399.
8. Owada, K., Ishikawa, K., Toru, S., Ishida, G., Gomyoda, M., Tao, O., Noguchi, Y., Kitamura, K., Kondo, I., Noguchi, E., et al. (2005). A clinical, genetic, and neuropathologic study in a family with 16q-linked ADCA type III. Neurology *65*, 629–632.
9. Hellenbroich, Y., Bubel, S., Pawlack, H., Opitz, S., Vieregge, P., Schwinger, E., and Zühlke, C. (2003). Refinement of the spinocerebellar ataxia type 4 locus in a large German family and exclusion of CAG repeat expansions in this region. J. Neurol. *250*, 668–671.
10. Hellenbroich, Y., Gierga, K., Reusche, E., Schwinger, E., Deller, T., de Vos, R.A., Zühlke, C., and Rüb, U. (2006). Spinocerebellar ataxia type 4 (SCA4): Initial pathoanatomical study reveals widespread cerebellar and brainstem degeneration. J. Neural Transm. *113*, 829–843.
11. Hellenbroich, Y., Bernard, V., and Zühlke, C. (2008). Spinocerebellar ataxia type 4 and 16q22.1-linked Japanese ataxia are not allelic. J. Neurol. *255*, 612–613.
12. Ohata, T., Yoshida, K., Sakai, H., Hamanoue, H., Mizuguchi, T., Shimizu, Y., Okano, T., Takada, F., Ishikawa, K., Mizusawa, H., et al. (2006). A −16C>T substitution in the 5′ UTR of the puratrophin-1 gene is prevalent in autosomal dominant cerebellar ataxia in Nagano. J. Hum. Genet. *51*, 461–466.
13. Amino, T., Ishikawa, K., Toru, S., Ishiguro, T., Sato, N., Tsunemi, T., Murata, M., Kobayashi, K., Inazawa, J., Toda, T., et al. (2007). Redefining the disease locus of 16q22.1-linked autosomal dominant cerebellar ataxia. J. Hum. Genet. *52*, 643–649.
14. Ouyang, Y., Sakoe, K., Shimazaki, H., Namekawa, M., Ogawa, T., Ando, Y., Kawakami, T., Kaneko, J., Hasegawa, Y., Yoshizawa, K., et al. (2006). 16q-linked autosomal dominant cerebellar ataxia: A clinical and genetic study. J. Neurol. Sci. *247*, 180–186.
15. Kobayashi, K., Nakahori, Y., Miyake, M., Matsumura, K., Kondo-Iida, E., Nomura, Y., Segawa, M., Yoshioka, M., Saito, K., Osawa, M., et al. (1998). An ancient retrotransposal insertion causes Fukuyama-type congenital muscular dystrophy. Nature *394*, 388–392.

16. Li, M., Ishikawa, K., Toru, S., Tomimitsu, H., Takashima, M., Goto, J., Takiyama, Y., Sasaki, H., Imoto, I., Inazawa, J., et al. (2003). Physical map and haplotype analysis of 16q-linked autosomal dominant cerebellar ataxia (ADCA) type III in Japan. J. Hum. Genet. *48*, 111–118.
17. Hattori, M., Fujiyama, A., Taylor, T.D., Watanabe, H., Yada, T., Park, H.S., Toyoda, A., Ishii, K., Totoki, Y., Choi, D.K., et al. (2000). The DNA sequence of human chromosome 21. Nature *405*, 311–319.
18. Asakawa, S., Abe, I., Kudoh, Y., Kishi, N., Wang, Y., Kubota, R., Kudoh, J., Kawasaki, K., Minoshima, S., and Shimizu, N. (1997). Human BAC library: Construction and rapid screening. Gene *191*, 69–79.
19. Jin, H., Ishikawa, K., Tsunemi, T., Ishiguro, T., Amino, T., and Mizusawa, H. (2008). Analyses of copy number and mRNA expression level of the α-synuclein gene in multiple system atrophy. J. Med. Dent. Sci. *55*, 145–153.
20. Barrett, M.T., Scheffer, A., Ben-Dor, A., Sampas, N., Lipson, D., Kincaid, R., Tsang, P., Curry, B., Baird, K., Meltzer, P.S., et al. (2004). Comparative genomic hybridization using oligonucleotide microarrays and total genomic DNA. Proc. Natl. Acad. Sci. USA *101*, 17765–17770.
21. Hara, K., Shiga, A., Nozaki, H., Mitsui, J., Takahashi, Y., Ishiguro, H., Yomono, H., Kurisaki, H., Goto, J., Ikeuchi, T., et al. (2008). Total deletion and a missense mutation of *ITPR1* in Japanese SCA15 families. Neurology *71*, 547–551.
22. Moseley, M.L., Zu, T., Ikeda, Y., Gao, W., Mosemiller, A.K., Daughters, R.S., Chen, G., Weatherspoon, M.R., Clark, H.B., Ebner, T.J., et al. (2006). Bidirectional expression of CUG and CAG expansion transcripts and intranuclear polyglutamine inclusions in spinocerebellar ataxia type 8. Nat. Genet. *38*, 758–769.
23. Taneja, K.L., McCurrach, M., Scalling, M., Housman, D., and Singer, R.H. (1995). Foci of trinucleotide repeat transcripts in nuclei of myotonic dystrophy cells and tissues. J. Cell Biol. *128*, 995–1002.
24. Chiodi, I., Corioni, M., Giordano, M., Valgardsdottir, R., Ghigna, C., Cobianchi, F., Xu, R.M., Riva, S., and Biamonti, G. (2004). RNA recognition motif 2 directs the recruitment of SF2/ASF to nuclear stress bodies. Nucleic Acids Res. *32*, 4127–4136.
25. Batzer, M.A., Deininger, P.L., Hellmann-Blumberg, U., Jurka, J., Labuda, D., Rubin, C.M., Schmid, C.W., Zietkiewicz, E., and Zuckerkandl, E. (1996). Standardized nomenclature for Alu repeats. J. Mol. Evol. *42*, 3–6.
26. Cleary, J.D., and Pearson, C.E. (2003). The contribution of cis-elements to disease-associated repeat instability: Clinical and experimental evidence. Cytogenet. Genome Res. *100*, 25–55.
27. Liquori, C.L., Ricker, K., Moseley, M.L., Jacobsen, J.F., Kress, W., Naylor, S.L., Day, J.W., and Ranum, L.P. (2001). Myotonic dystrophy type 2 caused by a CCTG expansion in intron 1 of *ZNF9*. Science *293*, 864–867.
28. Rizzi, N., Denegri, M., Chiodi, I., Corioni, M., Valgardsdottir, R., Cobianchi, F., Riva, S., and Biamonti, G. (2004). Transcriptional activation of a constitutive heterochromatic domain of the human genome in response to heat shock. Mol. Biol. Cell *15*, 543–551.
29. Valgardsdottir, R., Chiodi, I., Giordano, M., Rossi, A., Bazzini, S., Ghigna, C., Riva, S., and Biamonti, G. (2008). Transcription of Satellite III non-coding RNAs is a general stress response in human cells. Nucleic Acids Res. *36*, 423–434.
30. Valgardsdottir, R., Chiodi, I., Giordano, M., Cobianchi, F., Riva, S., and Biamonti, G. (2005). Structural and functional characterization of noncoding repetitive RNAs transcribed in stressed human cells. Mol. Biol. Cell *16*, 2597–2604.
31. Jolly, C., and Lakhotia, S.C. (2006). Human sat III and Drosophila hsr omega transcripts: a common paradigm for regulation of nuclear RNA processing in stressed cells. Nucleic Acids Res. *34*, 5508–5514.
32. Liquori, C.L., Ikeda, Y., Weatherspoon, M., Ricker, K., Schoser, B.G., Dalton, J.C., Day, J.W., and Ranum, L.P. (2003). Myotonic dystrophy type 2: human founder haplotype and evolutionary conservation of the repeat tract. Am. J. Hum. Genet. *73*, 849–862.
33. Grady, D.L., Ratliff, R.L., Robinson, D.L., McCanlies, E.C., Meyne, J., and Moyzis, R.K. (1992). Highly conserved repetitive DNA sequences are present at human centromeres. Proc. Natl. Acad. Sci. USA *89*, 1695–1699.
34. Scott, H.S., Kudoh, J., Wattenhofer, M., Shibuya, K., Berry, A., Chrast, R., Guipponi, M., Wang, J., Kawasaki, K., Asakawa, S., et al. (2001). Insertion of beta-satellite repeats identifies a transmembrane protease causing both congenital and childhood onset autosomal recessive deafness. Nat. Genet. *27*, 59–63.
35. Tassone, F., Iwahashi, C., and Hagerman, P.J. (2004). FMR1 RNA within the intranuclear inclusions of fragile X-associated tremor/ataxia syndrome (FXTAS). RNA Biol. *1*, 103–105.
36. Rudnicki, D.D., Holmes, S.E., Lin, M.W., Thornton, C.A., Ross, C.A., and Margolis, R.L. (2007). Huntington's disease-like 2 is associated with CUG repeat-containing RNA foci. Ann. Neurol. *61*, 272–282.
37. Iwahashi, C.K., Yasui, D.H., An, H.J., Greco, C.M., Tassone, F., Nannen, K., Babineau, B., Lebrilla, C.B., Hagerman, R.J., and Hagerman, P.J. (2006). Protein composition of the intranuclear inclusions of FXTAS. Brain *129*, 256–271.
38. Cooper, T.A., Wan, L., and Dreyfuss, G. (2009). RNA and disease. Cell *136*, 777–793.
39. Longman, D., Johnstone, I.L., and Caceres, J.F. (2000). Functional characterization of SR and SR-related gene in *Caenorhabditis elegans*. EMBO J. *19*, 1625–1637.
40. Kanadia, R.N., Clark, V.E., Punzo, C., Trimarchi, J.M., and Cepko, C.L. (2008). Temporal requirement of the alternative-splicing factor Sfrs1 for the survival of retinal neurons. Development *135*, 3923–3933.
41. Sanford, J.R., Wang, X., Mort, M., Vanduyn, N., Cooper, D.M., Mooney, S.D., Edenberg, H.J., and Liu, Y. (2009). Splicing factor SFRS1 recognizes a functionally diverse landscape of RNA transcripts. Genome Res. *19*, 381–394.
42. Sengupta, S., and Lakhotia, S.C. (2006). Altered expressions of the noncoding *hsr-ω* gene enhances poly-Q-induced neurotoxicity in *Drosophila*. RNA Biol. *3*, 28–35.

Glycobiology vol. 20 no. 1 pp. 99–106, 2010
doi:10.1093/glycob/cwp152
Advance Access publication on September 23, 2009

Protective effect of *N*-glycan bisecting GlcNAc residues on β-amyloid production in Alzheimer's disease

Keiko Akasaka-Manya[2], Hiroshi Manya[2], Yoko Sakurai[2], Boguslaw S Wojczyk[3], Yasunori Kozutsumi[4], Yuko Saito[5], Naoyuki Taniguchi[6], Shigeo Murayama[5], Steven L Spitalnik[3], and Tamao Endo[1,2]

[2]Department of Glycobiology, Tokyo Metropolitan Institute of Gerontology, Foundation for Research on Aging and Promotion of Human Welfare, Itabashi-ku, Tokyo 173-0015, Japan; [3]Department of Pathology and Cell Biology, Columbia University Medical Center, New York, NY 10032, USA; [4]Laboratory of Membrane Biochemistry and Biophysics, Graduate School of Biostudies, Kyoto University, Sakyo-ku, Kyoto, 606-8501; [5]Department of Neuropathology, Tokyo Metropolitan Institute of Gerontology, Foundation for Research on Aging and Promotion of Human Welfare, Itabashi-ku, Tokyo 173-0015; and [6]Department of Disease Glycomics, The Institute of Scientific and Industrial Research, Osaka University, Ibaraki, Osaka 565-0047, Japan

Received on August 4, 2009; revised on September 14, 2009; accepted on September 15, 2009

Alteration of glycoprotein glycans often changes various properties of the target glycoprotein and contributes to a wide variety of diseases. Here, we focused on the *N*-glycans of amyloid precursor protein whose cleaved fragment, β-amyloid, is thought to cause much of the pathology of Alzheimer's disease (AD). We previously determined the *N*-glycan structures of normal and mutant amyloid precursor proteins (the Swedish type and the London type). In comparison with normal amyloid precursor protein, mutant amyloid precursor proteins had higher contents of bisecting GlcNAc residues. Because *N*-acetylglucosaminyltransferase III (GnT-III) is the glycosyltransferase responsible for synthesizing a bisecting GlcNAc residue, the current report measured GnT-III mRNA expression levels in the brains of AD patients. Interestingly, GnT-III mRNA expression was increased in AD brains. Furthermore, β-amyloid treatment increased GnT-III mRNA expression in Neuro2a mouse neuroblastoma cells. We then examined the influence of bisecting GlcNAc on the production of β-amyloid. Both β-amyloid 40 and β-amyloid 42 were significantly decreased in GnT-III-transfected cells. When secretase activities were analyzed in GnT-III transfectant cells, α-secretase activity was increased. Taken together, these results suggest that upregulation of GnT-III in AD brains may represent an adaptive response to protect them from additional β-amyloid production.

Keywords: Alzheimer's disease/amyloid precursor protein/bisecting GlcNAc/*N*-glycan

Introduction

Alzheimer's disease (AD) is a progressive neurodegenerative disorder characterized by global cognitive decline involving memory, orientation, judgment, and reasoning. The presence of extracellular senile plaques is one of the classical characteristics of AD pathology. β-Amyloid (Aβ), the major component of senile plaques, is a cleaved fragment of a membrane-spanning glycoprotein, amyloid precursor protein (APP). APP requires cleavage by the β- and γ-secretases to release soluble Aβ. In contrast, α-secretase cleaves APP within the Aβ sequence and prevents the generation of Aβ. Indeed, α-secretase competes with β-secretase for APP processing in the trans-Golgi network (Skovronsky et al. 2000). According to the "amyloid cascade hypothesis," the abnormal accumulation of Aβ leads to neurodegenerative processes, finally resulting in neuronal death. Two types of Aβ are produced depending on the γ-secretase cleavage site: Aβ40 and Aβ42. Aβ42 is a minor form of Aβ but has a greater tendency to produce insoluble deposits and is a major component of senile plaques.

Glycoproteins glycans affect protein stability, conformation, cellular localization, and trafficking (Wang et al. 2005; Ohtsubo and Marth 2006). APP undergoes several posttranslational modifications including *N*- and *O*-linked glycosylation (Weidemann et al. 1989; Tomita et al. 1998; Sato et al. 1999). Core *N*-glycosylation and *N*-glycan processing modulate the synthesis and expression of APP (Pahlsson et al. 1992; Saito et al. 1995; Yazaki et al. 1996). In addition, sialylation of APP *N*-glycans enhanced secretion of its metabolites (Nakagawa et al. 2006). These studies suggest that *N*-glycosylation status may affect the APP metabolic pathway; however, much remains unknown.

We previously determined the *N*-glycan structures of normal and mutant APPs (i.e., the Swedish and London types) (Akasaka-Manya et al. 2008). The Swedish type mutation (Lys595/Met596 to Asn/Leu) increases Aβ42 secretion by 6- to 7-fold (Citron et al. 1992) and the London type mutation (Val642 to Phe) doubles the ratio of secreted Aβ42 to Aβ40 (Suzuki et al. 1994; Price et al. 1998; Sinha and Lieberburg 1999). When the *N*-glycan structures of these mutant APPs were analyzed, we found an increased content of bisecting GlcNAc residues. This prompted us to study the expression levels of β1,4-*N*-acetylglucosaminyltransferase III (GnT-III) in the brains of AD patients because GnT-III is the glycosyltransferase responsible for adding bisecting GlcNAc during *N*-glycan processing (Nishikawa et al. 1992) (Figure 1). The presence of bisecting GlcNAc on individual *N*-glycans prevents the subsequent actions of several glycosyltransferases, including α-mannosidase II, GnT-II, GnT-IV, and GnT-V (Narasimhan 1982; Schachter et al. 1983; Schachter 1986). Thus, attachment of bisecting GlcNAc can significantly alter the types *N*-glycan structures that

[1]To whom correspondence should be addressed: Tel: +81-3-3964-3241 ext. 3080; Fax: +81-3-3579-4776; e-mail: endo@tmig.or.jp

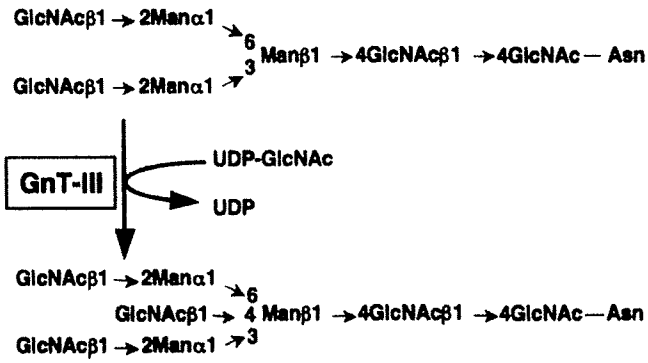

Fig. 1. Bisecting GlcNAc residues in *N*-glycans are synthesized by GnT-III.

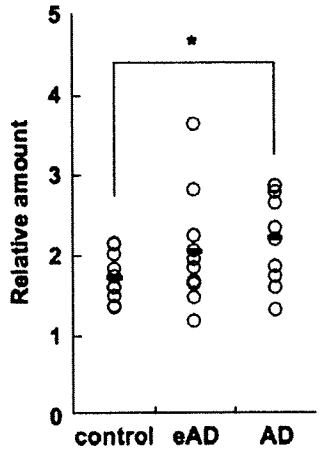

Fig. 2. Quantitative real-time RT-PCR analysis of *GnT-III* mRNA expression in brains of AD patients. Relative amounts of *GnT-III* mRNA were determined in 10 eAD patients, 10 AD patients, and 10 control subjects. All reactions were performed in triplicate and the open circles indicate average values for each individual brain sample. Each horizontal bar indicates the average value of the 10 subjects in that category. Statistically significant differences were identified using the Student's *t*-test ($P = 0.025$) and indicated with an asterisk.

are synthesized. Given the important biological functions of GnT-III (Gu and Taniguchi 2004), we examined the effects of the bisecting GlcNAc on Aβ production and on the activity of the various secretases responsible for Aβ production.

Results

GnT-III mRNA expression in the brains of AD patients

GnT-III catalyzes the transfer of GlcNAc to a core β-mannose residue, producing a bisecting GlcNAc (Wilson et al. 1976; Narasimhan 1982; Nishikawa et al. 1992). To investigate whether GnT-III levels are altered in AD, we measured the amount of *GnT-III* mRNA in the brains of AD patients by quantitative real-time RT-PCR. Preparation of total RNA from non-AD (control), early-stage AD (eAD), or AD brains and real-time RT-PCR analysis was performed as described in *Material and Methods*. As shown in Figure 2, the expression level of *GnT-III* mRNA was significantly increased in AD brains as compared to controls (mean relative amount of control, 1.74; standard deviation (SD), ± 0.28; mean relative amount of AD, 2.23; SD, ± 0.54; $P = 0.025$, Student's *t*-test). However, there was no statistically significant difference in *GnT-III* mRNA levels when comparing eAD brains to controls (mean relative amount of eAD, 2.06; SD, ± 0.68, $P = 0.21$, Student's *t*-test), or when comparing eAD brains to AD brains ($P = 0.56$, Student's *t*-test). Taken together, these results suggest that *GnT-III* mRNA expression increases with disease progression. Therefore, it is conceivable that the number of *N*-glycans having a bisecting GlcNAc residue is increased in AD brains.

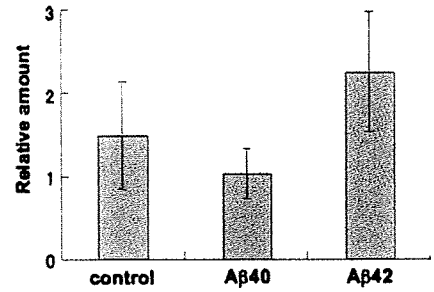

Fig. 3. Relative levels of *GnT-III* mRNA expression after incubation with Aβ. All reactions were performed in quadruplicate. Aβ40 or Aβ42 was added to Neuro2a cell culture medium at a final concentration of 2 μg/mL. After 48 h incubation, cells were harvested for RNA preparation followed by quantitative real-time RT-PCR. Average values ± 1 SD are shown.

Aβ42 exposure enhances GnT-III expression

We examined whether incubation with Aβ40 or Aβ42 affected *GnT-III* mRNA expression levels. Thus, after Aβ40 or Aβ42 was added to the culture media of Neuro2a cells, *GnT-III* expression level was analyzed by quantitative real-time RT-PCR (Figure 3). Compared to control cells (mean relative amount, 1.48; SD, ± 0.64), Aβ42 enhanced the *GnT-III* mRNA expression approximately 1.5-fold (mean relative amount, 2.24; SD, ± 0.72); in contrast, Aβ40 decreased the *GnT-III* expression (mean relative amount, 1.02; SD, ± 0.3). These results indicate that Aβ42, but not Aβ40, enhances GnT-III mRNA expression.

Effect of GnT-III on APP processing

According to our prior (Akasaka-Manya et al. 2008) and current (Figure 2) studies, it is likely that increased *GnT-III* mRNA levels increase the number of *N*-glycans having a bisecting GlcNAc residue. Therefore, we prepared stable transfectants of Neuro2a mouse neuroblastoma cells that express GnT-III by using an expression plasmid encoding *GnT-III*. The microsomal membrane fraction from the transfected cells was used as an enzyme source to measure GnT-III activity (Figure 4A). GnT-III activity was significantly increased in cells transfected with *GnT-III* (32.1 pmol/min/mg) as compared to cells transfected with the "empty" pCXN2 vector (mock transfectant, 0.1 pmol/min/mg). As expected, the intensity of staining by the *Phaseolus vulgaris* lectin E_4 ($PHA\text{-}E_4$), which specifically recognizes bisecting GlcNAc residues (Yamashita et al. 1983), was enhanced in cellular proteins prepared from *GnT-III*-transfected cells (Figure 4B), demonstrating that these proteins have a higher content of bisecting GlcNAc residues. There were no significant differences in the expression levels of membrane-bound APP and secreted APP (sAPP) (Figure 4C, upper-left panel and upper-right

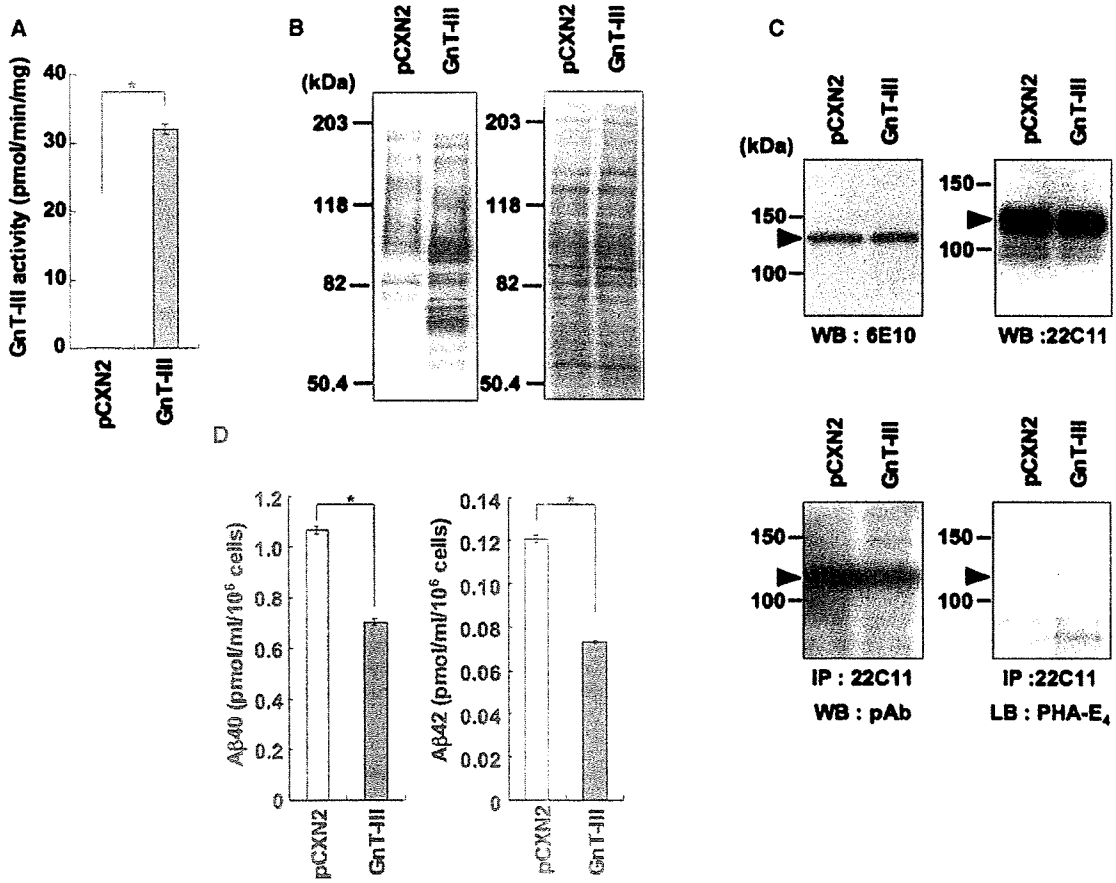

Fig. 4. Overexpression of *GnT-III* mRNA induces an increase in bisecting GlcNAc residues on cellular proteins and a decrease in Aβ secretion. (**A**) GnT-III activities of Neuro2a cells transfected with a *GnT-III* expression vector or an empty vector (pCXN2). Average values ± 1 SD of three independent experiments are shown. Asterisks indicate statistically significant differences ($P < 0.01$, Student's *t*-test). (**B**) Lectin (PHA-E_4) blot analysis of microsomal fraction of Neuro2a cells transfected with a *GnT-III* expression vector or an empty vector (pCXN2). Elevation of the bisecting GlcNAc modification was observed in *GnT-III*-transfected cells. Right panel indicates protein-staining patterns by Coomasie brilliant blue (CBB). Molecular weight standards are shown on the left. (**C**) Western blot analysis of membrane-bound APP or secreted APP (sAPP) in culture supernatants of Neuro2a cells transfected with a *GnT-III* expression vector or an empty vector (pCXN2). Membrane-bound APP was detected with an anti-APP monoclonal antibody (6E10) (upper-left panel) and sAPP in culture supernatant with an anti-APP monoclonal antibody (22C11) (upper-right panel). sAPP was immunoprecipitated from culture supernatant with an anti-APP monoclonal antibody (22C11), and then detected on blots by either an anti-APP polyclonal antibody (pAb, lower-left panel) or by the PHA-E_4 lectin (lower-right panel). Black triangle indicates membrane-bound APP and gray triangles indicate sAPP. Molecular weight standards are shown on the left. (**D**) The effect of GnT-III overexpression on Aβ production by transfected Neuro2a cells. Concentrations of Aβ40 (left) and Aβ42 (right) in culture supernatants were determined by ELISA. The average values ± 1 SD of three independent experiments are shown. Asterisks indicate statistically significant differences ($P < 0.01$, Student's *t*-test). pCXN2: stable mock transfectant of Neuro2a cells; GnT-III: stable transfectant of Neuro2a cells expressing GnT-III.

panel, respectively), but the intensity of PHA-E_4 staining of sAPP was enhanced in cells transfected with *GnT-III* (Figure 4C, lower-right panel). These results demonstrate that APP secreted from *GnT-III*-transfected cells has a higher content of bisecting GlcNAc residues.

We then measured levels of Aβ secreted by Neuro2a cells expressing recombinant GnT-III (Figure 4D). The concentrations of Aβ40 and Aβ42 secreted from the mock transfectant were 1.08 pmol/mL/10^6cells and 0.12 pmol/mL/10^6cells, respectively. For the *GnT-III* transfectant, the concentrations of Aβ40 and Aβ42 were 0.69 pmol/mL/10^6cells and 0.07 pmol/mL/10^6cells, respectively; these were 36.2% and 42.7% lower than those from the mock transfectant. These statistically significant results indicate that increased cellular expression of GnT-III significantly downregulates the secretion of Aβ peptides.

Western blot analysis of secretases

Contrary to our expectations, increased modification of *N*-glycans by bisecting GlcNAc downregulated Aβ secretion (Figure 4D). At least two mechanisms by which increased bisecting GlcNAc could reduce Aβ production should be considered. One possibility is that increasing bisecting GlcNAc expression on APP affects the conformation of APP, changing its susceptibility to α-, β-, and/or γ-secretase, and/or the intracellular localization of APP. Another possibility is that increasing the bisecting GlcNAc content of the secretases affects their enzymatic activity. α-Secretase activity is encoded by two proteins: ADAM 10 (a disintegrin and metalloproteinase 10) and tumor necrosis factor-α converting enzyme (TACE or, equivalently, ADAM 17). TACE has six potential *N*-glycosylation sites (Moss et al. 1997). ADAM 10 has four potential *N*-glycosylation sites, and their *N*-glycans are crucial for processing, localization, and

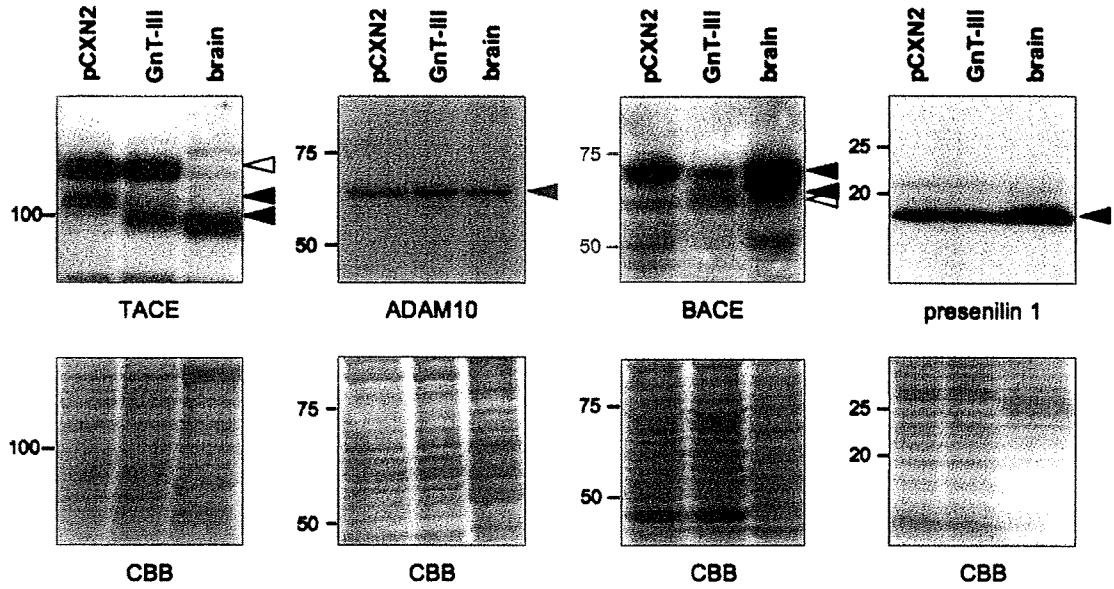

Fig. 5. Western blot analysis of various secretases (TACE, ADAM10, BACE, and presenilin) in *GnT-III*-transfected Neuro2a cells. For TACE and BACE, black and gray triangles indicate mature forms and white triangles indicate immature forms. For ADAM10 and presenilin 1, black triangles indicate the migration positions of ADAM10 and the C-terminal fragment of presenilin 1, respectively. Molecular weight standards are shown on the left. pCXN2: stable mock transfectant of Neuro2a cells; GnT-III: stable transfectant of Neuro2a cells expressing recombinant GnT-III; brain: mouse brain membrane fraction. Bottom figures indicate protein-staining patterns by CBB corresponding to each upper panel.

activity (Escrevente et al. 2008). BACE (β-site APP cleaving enzyme), which possesses β-secretase activity, has four potential *N*-glycosylation sites, three of them appear to be glycosylated (Charlwood et al. 2001). γ-Secretase is a protein complex consisting of presenilin, nicastrin, APH-1, and PEN-2. Nicastrin has 16 potential *N*-glycosylation sites, although inhibition of complex *N*-glycan processing does not affect γ-secretase activity (Herreman et al. 2003).

To clarify the mechanism(s) responsible for downregulating Aβ secretion, the expression levels of the secretases were measured. TACE is reported to change from an immature to a mature form (Milla et al. 1999; Schlondorff et al. 2000; Peiretti et al. 2003). Our Western blot analysis of TACE expressed by Neuro2a cells showed two major bands (Figure 5, left lane); results with proteins isolated from normal mouse brain are shown for comparison. The upper band (white triangle) corresponds to immature TACE bearing high-mannose *N*-glycans; the lower band corresponds to mature TACE (black triangle). Although two TACE bands were also observed in *GnT-III*-transfected Neuro2a cells (Figure 5, right lane), the mobility of mature TACE (gray triangle) from *GnT-III*-transfected cells was faster than that from the mock transfectant. As reported previously, this type of finding is a unique feature seen by introducing bisecting GlcNAc into glycoprotein *N*-glycans (Shigeta et al. 2006). In addition, the expression level of TACE in *GnT-III*-transfected cells was nearly the same as compared with mock transfectant. BACE is also reported to change from an immature form to a mature form (Benjannet et al. 2001; Schmechel et al. 2004). Our Western blot analysis of Neuro2a cells showed two BACE bands (Figure 5, left lane). The upper band corresponds to mature BACE (black triangle) and the lower to immature BACE (white triangle). An additional new band of intermediate mobility appeared in the *GnT-III*-transfected cells (Figure 5, gray triangle in the right lane). Interestingly, in the *GnT-III* transfectant, the molecular size and expression of BACE both decreased. In contrast, when comparing the mock transfectant with the *GnT-III* transfectant, no differences in the expression level or molecular size of ADAM 10 or the C-terminal fragment of presenilin 1 were seen (Thinakaran et al. 1996) (Figure 5). Taken together, these results suggest that changing the *N*-glycans of TACE and BACE may affect α- and β-secretase activities.

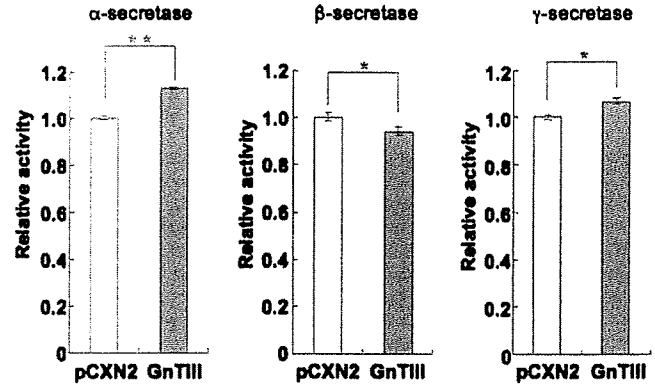

Fig. 6. Secretase activities in *GnT-III*-transfected Neuro2a cells. α-, β-, and γ-secretase activities (left, middle and right panels, respectively) were determined. For comparison, the fluorescence intensity of the pCXN2 transfectant was set to 1.0. The average percentages ± 1 SD of three independent experiments are shown. Asterisks indicate statistically significant differences (*$P < 0.01$, **$P = 0.0001$, Student's *t*-test).

Secretase assays

To examine the effect of *N*-glycan changes of TACE and BACE on enzymatic activity, we measured α- and β-secretase activities in *GnT-III* transfectants of Neuro2a cells. As shown in Figure 6, in the *GnT-III* transfectant, α-secretase activity (113% of the

activity of the control pCXN2 transfectant, $P = 0.0001$) was slightly upregulated, but β-secretase activity (97% of the pCXN2 transfectant, $P = 0.042$) was modestly downregulated. Because changes in γ-secretase activity may also affect Aβ production, its activity in *GnT-III*-transfected cells was measured; modest upregulation was observed (107% of the pCXN2 transfectant, $P = 0.015$). Taken together, the increased α-secretase activity and decreased β-secretase activity in the *GnT-III* transfectant were the most probable cause of the reduction in Aβ production shown in Figure 4D. Thus, these results suggest that changes in *N*-glycan of TACE and BACE affect their enzymatic activities and lead to downregulation of Aβ production.

Discussion

In previous studies, we described the *N*-glycan structures of APP695 produced by Chinese hamster ovary cells (Sato et al. 1999) and the C17.2 mouse neural stem cell line (Akasaka-Manya et al. 2008). Recombinant APP695 in both cell lines had sialylated bi- and triantennary complex-type *N*-glycans with fucosylated and nonfucosylated trimannosyl cores. However, only APP695 produced by C17.2 cells had *N*-glycans containing bisecting GlcNAc. This may be due to cell-type-specific differences in *N*-glycan processing that can be found with various recombinant glycoproteins (Kagawa et al. 1988; Cumming 1991). To determine whether mutations in the *APP* gene alter the structures of processed *N*-glycans, we expressed two mutant recombinant APPs (i.e., the Swedish type and the London type) in transfected C17.2 cells. Structural analysis of these *N*-glycans revealed that the two mutant APPs had higher contents of bisecting GlcNAc and core-fucose residues as compared to wild-type APP. These results clearly showed that these slight changes in amino acid sequence affected *N*-glycan processing.

The glycosyltransferase responsible for adding the bisecting GlcNAc residue is GnT-III (Wilson et al. 1976; Narasimhan 1982; Nishikawa et al. 1992). To examine whether *GnT-III* mRNA levels are related to the pathogenesis of sporadic AD, we examined this issue by quantitative real-time RT-PCR using brains of normal individuals and AD patients. As shown in Figure 2, *GnT-III* mRNA levels were significantly increased in the brains of AD patients. This upregulation may affect AD pathogenesis because significant differences were found in patients with an advanced stage of AD. Interestingly, incubation of Neuro2a cells with Aβ42 increased *GnT-III* gene expression levels (Figure 3). In a recent report (Fiala et al. 2007), exposure of normal peripheral blood mononuclear cells to Aβ peptide upregulated transcription of *GnT-III* and led to increased Aβ clearance by phagocytosis; interestingly, mononuclear cells isolated from AD patients exhibited downregulated *GnT-III* gene expression and were defective in phagocytosis of Aβ. Since upregulation of GnT-III expression was associated with enhanced phagocytosis of Aβ, an increment of GnT-III levels in mononuclear cells may lead to improved Aβ clearance. In contrast, as reported here, increased expression of GnT-III in Neuro2a cells downregulated Aβ production (Figure 4D), and *GnT-III* mRNA levels were increased in AD brains (Figure 2). Taken together, these results suggest that upregulation of GnT-III in neuronal cells may diminish Aβ production in AD brains. In addition, expression of GnT-III in neurons and monocytes may modulate Aβ accumulation by different mechanisms. That is, upregulation of GnT-III expression in monocytes may enhance Aβ clearance, and increased GnT-III expression in neuronal cells may inhibit Aβ production. Taken together, both responses may be adaptive, protective responses that inhibit the further progression of AD.

To evaluate the mechanism by which an increased number of bisecting GlcNAc residues could reduce Aβ production, several possibilities should be considered. As reported here, the APP secreted by *GnT-III*-transfected Neuro2a cells has a higher content of bisecting GlcNAc than that secreted by control cells (Figure 4C). The addition of bisecting GlcNAc may affect the conformation of APP, thereby leading to a change in its susceptibility to α-, β-, and/or γ-secretases. Alteration of glycoprotein glycans is known to affect various properties of a given protein including its susceptibility to various modifying enzymes. For example, organ-specific differential glycosylation of low-density lipoprotein receptor-related protein 1 (LRP1) alters its proteolytic cleavage by γ-secretase (May et al. 2003). In addition, increased sialylation of APP enhanced Aβ secretion (Nakagawa et al. 2006). Bisecting GlcNAc residues are also known to affect the branching and elongation of various *N*-glycans antennae (Narasimhan 1982; Schachter et al. 1983; Schachter 1986). Therefore, it is possible that increasing bisecting GlcNAc expression on APP leads to changes in the APP *N*-glycan structure, including less sialylation, which may alter it susceptibility to cleavage by individual secretases (Fukuta et al. 2000; Koyota et al. 2001). Furthermore, because changing the *N*-glycan structure can alter intracellular glycoprotein localization, it is possible that bisecting GlcNAc affects APP trafficking and, thereby, its susceptibility to secretases. For example, in cells that overexpress GnT-III, cell surface turnover of E-cadherin is delayed (Yoshimura et al. 1996). In contrast, the cell surface expression of epidermal growth factor receptor is reduced in GnT-III overexpressing cells (Rebbaa et al. 1997). In addition, APP localization and trafficking vary according to its glycan modifications (McFarlane et al. 1999).

Another possibility is that increasing the bisecting GlcNAc content of the secretases affects their enzymatic activity. For example, glycosylation is known to play a critical role in maintaining the enzymatic activity of β-secretase (Charlwood et al. 2001). In that study, baculovirus-expressed β-secretase, which only has high-mannose-type *N*-glycans, exhibits only ~50% of the activity found when the enzyme is expressed by mammalian cells, when it has complex-type *N*-glycans (Charlwood et al. 2001). To investigate this issue, we measured secretase activities in *GnT-III*-transfected cells; α- and β-secretase activities were significantly increased and decreased, respectively (Figure 6). By Western blot analysis, the *N*-glycan structures of TACE and BACE are altered (Figure 5), perhaps explaining the changes in their enzymatic activities. In a previous study (Skovronsky et al. 2001), TACE-expressing neurons often colocalized with Aβ plaques. Our results showed that GnT-III expression was increased in AD brains (Figure 2) and that increases in GnT-III might decrease BACE expression (Figure 6). Taken together, it is likely that upregulation of GnT-III in AD brains induces changes in the APP processing enzymes, TACE and BACE, which may inhibit Aβ formation. Although the detailed mechanisms are not yet clear, this increased expression of GnT-III may homeostatically partially protect AD brains from further Aβ production.

Bisected *N*-glycans play important roles in neurological function in vitro and in vivo. For example, bisecting GlcNAc

regulated serum depletion-induced neuritogenesis (Shigeta et al. 2006). In addition, truncated, inactive GnT-III induced abnormal neurological phenotypes in mice (Bhattacharyya et al. 2002). As another example, changes in bisected *N*-glycans may be related to the pathogenesis of prion disease (Rudd et al. 1999). Therefore, further studies are required to understand the precise physiological and pathological roles of bisecting GlcNAc in brain development and function.

In summary, based on the current results, we propose that high expression of GnT-III in human AD brains reduces Aβ production and protects against further deterioration of neurological function during this disease process. Therefore, compounds that upregulate the expression of bisecting *N*-glycans may provide a novel therapeutic approach toward preventing or ameliorating AD.

Material and methods

Patients and controls

Human brain tissues were obtained from the Brain Bank for Aging Research (BBAR), which consists of consecutive autopsy cases from a general geriatric hospital with informed consent obtained from the relatives for each autopsy. The brains were handled using the BBAR protocol described previously (Fumimura et al. 2007). In brief, half of the brain was serially sections into 7 mm slices, snap-frozen using powdered dry ice, and stored at −80°C. To minimize RNA degradation, samples with the shortest postmortem intervals were selected for study. Two grams of frozen gray matter were sampled from the temporal pole of 10 cases each with AD, eAD, and age-matched normal controls. The diagnosis of AD was based on the BBAR criteria (Hughes et al. 1982; Murayama and Saito 2004), as follows: (1) clinical dementia rating (Hughes et al. 1982) ≥ 1; (2) Braak's senile plaque stage equal to C; and (3) the Braak's neurofibrillary tangle stage ≥ IV. The diagnosis of eAD was based on the following criteria: (1) clinical dementia rating, either 0 or 0.5; (2) Braak's senile plaque stage ≥ B; and (3) Braak's neurofibirillary tangle stage ≥ III. The criteria for designating brains as coming from normal controls included a clinical dementia rating of 0, Braak's senile plaque stage 0, and Braak's neurofibrillary tangle stage ≤ II. The age of the selected AD cases ranged from 79 to 98 years old (average of 88.2 years), and the postmortem interval from 1.8 to 17.7 h (average of 7.1 h). The age of the eAD cases ranged between 76 and 96 years (average of 90.3 years), and the postmortem interval between 1.2 and 39.9 h (average of 9.6 h). The age of the normal controls ranged from 68 to 86 years (average of 75.8 years), and the postmortem interval ranged from 1.5 to 29.1 h (average of 7.4 h). This study was approved by the Internal Review Board of Tokyo Metropolitan Institute of Gerontology and of Tokyo Metropolitan Geriatric Hospital.

Real-time RT-PCR analysis

Total RNA was isolated from a portion of each patient's brain using the guanidinium thiocyanate method with TRIzol (Invitrogen Corp., Carlsbad, CA), following the manufacturer's instructions. The integrity of the isolated total RNA was confirmed using an Agilent 2100 bioanalyzer (Agilent Technologies, Inc., Santa Clara, CA). Total RNA from Neuro2a cells was isolated using ISOGEN (Nippon Gene Co., Ltd, Tokyo, Japan), following the manufacturer's instructions. First-strand cDNAs were synthesized using 5 μg of total RNA, SuperScript II RNase H⁻ Reverse Transcriptase, and random primers (Invitrogen). The relative quantification of target mRNA was determined using a TaqMan real-time RT-PCR assay on a 7300 Fast Real-Time PCR System (Applied Biosystems, Foster City, CA), following the manufacturer's instructions using the TaqMan Universal PCR Master Mix and TaqMan Gene Expression Assays (i.e., a mixture of designed primers and TaqMan probes, Applied Biosystems): *GnT-III*, Hs02379589_s1; endogenous control, the TaqMan Ribosomal RNA Control Reagents VIC Probe. 18S rRNA was used as normalization control.

Cell culture and expression of GnT-III

Neuro2a mouse neuroblastoma cells were maintained in a mixture of Dulbecco's modified Eagle's medium and OptiMEM (1:1, v/v, Invitrogen) supplemented with 5% fetal bovine serum (Invitrogen), 2 mM L-glutamine, 100 units/mL penicillin, and 50 μg/mL streptomycin at 37°C in a 5% CO_2 atmosphere. The pCXN2-rat-*GnT-III* expression plasmid was described previously (Kitada et al. 2001). This plasmid was transfected into Neuro2a cells using Lipofectamine PLUS reagent (Invitrogen) according to the manufacturer's instructions. Stable transfectants were selected with G418 (Invitrogen) at 1 mg/mL. The culture supernatants of these transfectants were collected after 24 h incubation in Dulbecco's modified Eagle's medium:OptiMEM (1:1, v/v) supplemented with 0.2% fetal bovine serum. The cells were homogenized in 10 mM Tris-HCl, pH 7.4, 1 mM EDTA, 250 mM sucrose, 1 mM dithiothreitol, with protease inhibitor mixture (3 μg/mL pepstatin A, 1 μg/mL leupeptin, 1 mM benzamidine-HCl, 1 mM PMSF). After centrifugation at 900 × *g* for 10 min, the supernatant was centrifuged at 100,000 × *g* for 1 h; the pellet was used as the microsomal fraction. Protein concentration was determined by BCA assay (Thermo Fisher Scientific Inc., Waltham, MA).

Aβ treatment of Neuro2a cells was performed as follows: Aβ40 and Aβ42 were each purchased from PEPTIDE INSTITUTE, INC. (Osaka, Japan) and dissolved in H_2O. Aβ40 or Aβ42 were added to culture medium at a final concentration of 2 μg/mL. Cells were cultured for 48 h and harvested for RNA preparation followed by real-time RT-PCR.

Preparation of mouse brain membrane fraction

Brains were obtained from 4-week-old C57BL/6 mice, and homogenized with 9 volumes (weight/volume) of 10 mM Tris-HCl, pH 7.4, 1 mM EDTA, 250 mM sucrose. After centrifugation at 900 × *g* for 10 min, the supernatant was centrifuged at 100,000 × *g* for 1 h; the pellet was used as the microsomal membrane fraction. Protein concentration was determined by BCA assay. All experimental procedures using laboratory animals were approved by the Animal Care and Use Committee of Tokyo Metropolitan Institute of Gerontology.

Assay for GnT-III activity

GnT-III activity was measured using a modification of a previously reported method (Taniguchi et al. 1989). The enzyme assay mixture, containing 125 mM MES buffer (pH 6.25), 200 mM GlcNAc, 10 mM $MnCl_2$, 20 mM UDP-GlcNAc, 0.5% Triton X-100, 10 μM of 2-aminobenzamide-labeled [GlcNAcβ1-2Manα1-6 (GlcNAcβ1-2Manα1-3) Manβ1-4Glc

NAcβ1-4GlcNAc] (ProZyme, Leandro, CA), and cell homogenate were incubated at 37°C for 1 h. After boiling for 3 min to stop the reaction, the mixture was subjected to reversed-phase HPLC using a Cosmosil 5C18-AR column (Nacalai Tesque, Kyoto, Japan), which was equilibrated with the 100 mM ammonium acetate buffer, pH 4.0, and eluted with a gradient of 1-butanol (0.25–1% butanol) over 120 min at a flow rate of 1 mL/min at 55°C.

Immunoprecipitation

For APP immunoprecipitation, culture supernatants were mixed with an anti-APP monoclonal antibody (22C11, Millipore, Billerica, MA). After incubation at 4°C for 2 h, Protein G-coupled Sepharose-4B beads (GE Healthcare UK Ltd., Buckinghamshire, England) were added and the mixture rotated at 4°C for 2 h. The beads were washed three times with PBS and suspended in the sample buffer. Immunoprecipitated proteins were recovered by boiling for 3 min and then subjected to Western blot and lectin blot analyses.

Western blot analysis

Proteins were separated by SDS–PAGE (for TACE, a 5–10% gradient gel; for APP, BACE, and ADAM 10, a 7.5% gel; for presenilin 1, a 12.5% gel) and transferred to a PVDF membrane. The membrane, after blocking in PBS containing 5% skim milk and 0.05% Tween 20, was incubated with an anti-APP polyclonal antibody (Millipore, Billerica, MA) or an anti-APP monoclonal antibody (6E10, Signet laboratories, Dedham, MA). The membrane was then incubated with anti-rabbit IgG conjugated with horseradish peroxidase (GE Healthcare). Antibody-bound proteins were visualized using an ECL kit (GE Healthcare).

Secretases in the microsomal fractions were visualized after separation by SDS–PAGE using anti-TACE polyclonal antibody (Thermo Fisher Scientific), anti-ADAM10 antibody, anti-presenilin 1 antibody, and anti-BACE antibody (Abcam, Cambridge, England).

Lectin blot analysis

Immunoprecipitated proteins were separated by SDS–PAGE and transferred to a PVDF membrane. After blocking with 3% bovine serum albumin (BSA, Nacalai Tesque) in 10 mM Tris-HCl (pH 7.4) containing 140 mM NaCl, 1 mM $CaCl_2$, 1 mM $MgCl_2$, 1 mM $MnCl_2$, and 0.05% Tween 20 (TBS-T), the membrane was incubated with biotin-conjugated PHA-E_4 (Seikagaku Corporation, Tokyo, Japan) in TBS-T containing 1% BSA. After treating the membrane with the Vectastain ABC kit (Vector, Burlingame, CA), lectin-bound proteins were visualized with an ECL kit.

Quantification of soluble Aβ by sandwich ELISA

Culture supernatants were subjected to enzyme-linked immunosorbent assay (ELISA) using the Human/Rat β-Amyloid 40 ELISA kit II and the Human/Rat β-Amyloid 42 ELISA kit High Sensitive (Wako Pure Chemical Industries, Ltd., Osaka, Japan) according to manufacturer's instructions.

Secretase assays

Secretase enzymatic assays were performed using the α-secretase assay kit, β-secretase assay kit, and γ-secretase assay kit (R & D Systems, Inc., Minneapolis, MN), according to manufacturer's instructions. Briefly, cultured Neuro2a cells were harvested and cell numbers counted. Cells were lysed with the extraction buffer and used as an enzyme source for the assay. An APP peptide conjugated to fluorescent reporter and quencher was used as the substrate. The protein content of cell lysates was determined by BCA assay and secretase activities were normalized to protein concentration.

Funding

The Japan Society for the Promotion of Science (20390031).

Acknowledgements

We thank Ms. Harumi Yamamoto and Ms. Reiko Fujinawa for technical assistance.

Conflict of interest statement

None declared.

Abbreviations

Aβ, β-amyloid; AD, Alzheimer's disease; ADAM, a disintegrin and metalloprotease; APP, amyloid precursor protein; BACE, β-site APP-cleaving enzyme; eAD, early-stage AD; GnT, *N*-acetylglucosaminyltransferase; TACE, tumor necrosis factor-α-converting enzyme.

References

Akasaka-Manya K, Manya H, Sakurai Y, Wojczyk BS, Spitalnik SL, Endo T. 2008. Increased bisecting and core-fucosylated *N*-glycans on mutant human amyloid precursor proteins. *Glycoconj J.* 25:775–786.

Benjannet S, Elagoz A, Wickham L, Mamarbachi M, Munzer JS, Basak A, Lazure C, Cromlish JA, Sisodia S, Checler F, et al. 2001. Post-translational processing of β-secretase (β-amyloid-converting enzyme) and its ectodomain shedding. The pro- and transmembrane/cytosolic domains affect its cellular activity and amyloid-β production. *J Biol Chem.* 276:10879–10887.

Bhattacharyya R, Bhaumik M, Raju TS, Stanley P. 2002. Truncated, inactive *N*-acetylglucosaminyltransferase III (GlcNAc-TIII) induces neurological and other traits absent in mice that lack GlcNAc-TIII. *J Biol Chem.* 277:26300–26309.

Charlwood J, Dingwall C, Matico R, Hussain I, Johanson K, Moore S, Powell DJ, Skehel JM, Ratcliffe S, Clarke B, et al. 2001. Characterization of the glycosylation profiles of Alzheimer's β-secretase protein Asp-2 expressed in a variety of cell lines. *J Biol Chem.* 276:16739–16748.

Citron M, Oltersdorf T, Haass C, McConlogue L, Hung AY, Seubert P, Vigo-Pelfrey C, Lieberburg I, Selkoe DJ. 1992. Mutation of the β-amyloid precursor protein in familial Alzheimer's disease increases β-protein production. *Nature.* 360:672–674.

Cumming DA. 1991. Glycosylation of recombinant protein therapeutics: Control and functional implications. *Glycobiology.* 1:115–130.

Escrevente C, Morais VA, Keller S, Soares CM, Altevogt P, Costa J. 2008. Functional role of *N*-glycosylation from ADAM10 in processing, localization and activity of the enzyme. *Biochim Biophys Acta.* 1780:905–913.

Fiala M, Liu PT, Espinosa-Jeffrey A, Rosenthal MJ, Bernard G, Ringman JM, Sayre J, Zhang L, Zaghi J, Dejbakhsh S, et al. 2007. Innate immunity and transcription of MGAT-III and Toll-like receptors in Alzheimer's disease patients are improved by bisdemethoxycurcumin. *Proc Natl Acad Sci USA.* 104:12849–12854.

Fukuta K, Abe R, Yokomatsu T, Omae F, Asanagi M, Makino T. 2000. Control of bisecting GlcNAc addition to *N*-linked sugar chains. *J Biol Chem.* 275:23456–23461.

Fumimura Y, Ikemura M, Saito Y, Sengoku R, Kanemaru K, Sawabe M, Arai T, Ito G, Iwatsubo T, Fukayama M, et al. 2007. Analysis of the adrenal gland is useful for evaluating pathology of the peripheral autonomic nervous system in Lewy body disease. *J Neuropathol Exp Neurol.* 66:354–362.

Gu J, Taniguchi N. 2004. Regulation of integrin functions by *N*-glycans. *Glycoconj J.* 21:9–15.

Herreman A, Van Gassen G, Bentahir M, Nyabi O, Craessaerts K, Mueller U, Annaert W, De Strooper B. 2003. γ-Secretase activity requires the presenilin-dependent trafficking of nicastrin through the Golgi apparatus but not its complex glycosylation. *J Cell Sci.* 116:1127–1136.

Hughes CP, Berg L, Danziger WL, Coben LA, Martin RL. 1982. A new clinical scale for the staging of dementia. *Br J Psychiatry.* 140:566–572.

Kagawa Y, Takasaki S, Utsumi J, Hosoi K, Shimizu H, Kochibe N, Kobata A. 1988. Comparative study of the asparagine-linked sugar chains of natural human interferon-β 1 and recombinant human interferon-β 1 produced by three different mammalian cells. *J Biol Chem.* 263:17508–17515.

Kitada T, Miyoshi E, Noda K, Higashiyama S, Ihara H, Matsuura N, Hayashi N, Kawata S, Matsuzawa Y, Taniguchi N. 2001. The addition of bisecting *N*-acetylglucosamine residues to E-cadherin down-regulates the tyrosine phosphorylation of β-catenin. *J Biol Chem.* 276:475–480.

Koyota S, Ikeda Y, Miyagawa S, Ihara H, Koma M, Honke K, Shirakura R, Taniguchi N. 2001. Down-regulation of the α-Gal epitope expression in *N*-glycans of swine endothelial cells by transfection with the *N*-acetylglucosaminyltransferase III gene. Modulation of the biosynthesis of terminal structures by a bisecting GlcNAc. *J Biol Chem.* 276:32867–32874.

May P, Bock HH, Nimpf J, Herz J. 2003. Differential glycosylation regulates processing of lipoprotein receptors by γ-secretase. *J Biol Chem.* 278:37386–37392.

McFarlane I, Georgopoulou N, Coughlan CM, Gillian AM, Breen KC. 1999. The role of the protein glycosylation state in the control of cellular transport of the amyloid β precursor protein. *Neuroscience.* 90:15–25.

Milla ME, Leesnitzer MA, Moss ML, Clay WC, Carter HL, Miller AB, Su JL, Lambert MH, Willard DH, Sheeley DM, et al. 1999. Specific sequence elements are required for the expression of functional tumor necrosis factor-α-converting enzyme (TACE). *J Biol Chem.* 274:30563–30570.

Moss ML, Jin SL, Milla ME, Bickett DM, Burkhart W, Carter HL, Chen WJ, Clay WC, Didsbury JR, Hassler D, et al. 1997. Cloning of a disintegrin metalloproteinase that processes precursor tumour-necrosis factor-α. *Nature.* 385: 733–736.

Murayama S, Saito Y. 2004. Neuropathological diagnostic criteria for Alzheimer's disease. *Neuropathology.* 24:254–260.

Nakagawa K, Kitazume S, Oka R, Maruyama K, Saido TC, Sato Y, Endo T, Hashimoto Y. 2006. Sialylation enhances the secretion of neurotoxic amyloid-β peptides. *J Neurochem.* 96:924–933.

Narasimhan S. 1982. Control of glycoprotein synthesis. UDP-GlcNAc:glycopeptide β 4-*N*-acetylglucosaminyltransferase III, an enzyme in hen oviduct which adds GlcNAc in β 1–4 linkage to the beta-linked mannose of the trimannosyl core of *N*-glycosyl oligosaccharides. *J Biol Chem.* 257:10235–10242.

Nishikawa A, Ihara Y, Hatakeyama M, Kangawa K, Taniguchi N. 1992. Purification, cDNA cloning, and expression of UDP-*N*-acetylglucosamine: β-D-mannoside β-1,4*N*-acetylglucosaminyltransferase III from rat kidney. *J Biol Chem.* 267:18199–18204.

Ohtsubo K, Marth JD. 2006. Glycosylation in cellular mechanisms of health and disease. *Cell.* 126:855–867.

Pahlsson P, Shakin-Eshleman SH, Spitalnik SL. 1992. *N*-Linked glycosylation of β-amyloid precursor protein. *Biochem Biophys Res Commun.* 189:1667–1673.

Peiretti F, Canault M, Deprez-Beauclair P, Berthet V, Bonardo B, Juhan-Vague I, Nalbone G. 2003. Intracellular maturation and transport of tumor necrosis factor α converting enzyme. *Exp Cell Res.* 285:278–285.

Price DL, Sisodia SS, Borchelt DR. 1998. Genetic neurodegenerative diseases: The human illness and transgenic models. *Science.* 282:1079–1083.

Rebbaa A, Yamamoto H, Saito T, Meuillet E, Kim P, Kersey DS, Bremer EG, Taniguchi N, Moskal JR. 1997. Gene transfection-mediated overexpression of β 1,4-*N*-acetylglucosamine bisecting oligosaccharides in glioma cell line U373 MG inhibits epidermal growth factor receptor function. *J Biol Chem.* 272:9275–9279.

Rudd PM, Endo T, Colominas C, Groth D, Wheeler SF, Harvey DJ, Wormald MR, Serban H, Prusiner SB, Kobata A, et al. 1999. Glycosylation differences between the normal and pathogenic prion protein isoforms. *Proc Natl Acad Sci USA.* 96:13044–13049.

Saito F, Tani A, Miyatake T, Yanagisawa K. 1995. *N*-Linked oligosaccharide of β-amyloid precursor protein (β APP) of C6 glioma cells: Putative regulatory role in β APP processing. *Biochem Biophys Res Commun.* 210:703–710.

Sato Y, Liu C, Wojczyk BS, Kobata A, Spitalnik SL, Endo T. 1999. Study of the sugar chains of recombinant human amyloid precursor protein produced by Chinese hamster ovary cells. *Biochim Biophys Acta.* 1472:344–358.

Schachter H. 1986. Biosynthetic controls that determine the branching and microheterogeneity of protein-bound oligosaccharides. *Biochem Cell Biol.* 64:163–181.

Schachter H, Narasimhan S, Gleeson P, Vella G. 1983. Control of branching during the biosynthesis of asparagine-linked oligosaccharides. *Can J Biochem Cell Biol.* 61:1049–1066.

Schlondorff J, Becherer JD, Blobel CP. 2000. Intracellular maturation and localization of the tumour necrosis factor α convertase (TACE). *Biochem J.* 347(Pt 1):131–138.

Schmechel A, Strauss M, Schlicksupp A, Pipkorn R, Haass C, Bayer TA, Multhaup G. 2004. Human BACE forms dimers and colocalizes with APP. *J Biol Chem.* 279:39710–39717.

Shigeta M, Shibukawa Y, Ihara H, Miyoshi E, Taniguchi N, Gu J. 2006. β 1,4-*N*-acetylglucosaminyltransferase III potentiates β1 integrin-mediated neuritogenesis induced by serum deprivation in Neuro2a cells. *Glycobiology.* 16:564–571.

Sinha S, Lieberburg I. 1999. Cellular mechanisms of β-amyloid production and secretion. *Proc Natl Acad Sci USA.* 96:11049–11053.

Skovronsky DM, Fath S, Lee VM, Milla ME. 2001. Neuronal localization of the TNFα converting enzyme (TACE) in brain tissue and its correlation to amyloid plaques. *J Neurobiol.* 49:40–46.

Skovronsky DM, Moore DB, Milla ME, Doms RW, Lee VM. 2000. Protein kinase C-dependent α-secretase competes with β-secretase for cleavage of amyloid-β precursor protein in the trans-Golgi network. *J Biol Chem.* 275:2568–2575.

Suzuki N, Cheung TT, Cai XD, Odaka A, Otvos L Jr, Eckman C, Golde TE, Younkin SG. 1994. An increased percentage of long amyloid β protein secreted by familial amyloid β protein precursor (β APP717) mutants. *Science.* 264:1336–1340.

Taniguchi N, Nishikawa A, Fujii S, Gu JG. 1989. Glycosyltransferase assays using pyridylaminated acceptors: *N*-acetylglucosaminyltransferase III, IV, and V. *Methods Enzymol.* 179:397–408.

Thinakaran G, Borchelt DR, Lee MK, Slunt HH, Spitzer L, Kim G, Ratovitsky T, Davenport F, Nordstedt C, Seeger M, et al. 1996. Endoproteolysis of presenilin 1 and accumulation of processed derivatives in vivo. *Neuron.* 17:181–190.

Tomita S, Kirino Y, Suzuki T. 1998. Cleavage of Alzheimer's amyloid precursor protein (APP) by secretases occurs after *O*-glycosylation of APP in the protein secretory pathway. Identification of intracellular compartments in which APP cleavage occurs without using toxic agents that interfere with protein metabolism. *J Biol Chem.* 273:6277–6284.

Wang X, Inoue S, Gu J, Miyoshi E, Noda K, Li W, Mizuno-Horikawa Y, Nakano M, Asahi M, Takahashi M, et al. 2005. Dysregulation of TGF-β1 receptor activation leads to abnormal lung development and emphysema-like phenotype in core fucose-deficient mice. *Proc Natl Acad Sci USA.* 102:15791–15796.

Weidemann A, Konig G, Bunke D, Fischer P, Salbaum JM, Masters CL, Beyreuther K. 1989. Identification, biogenesis, and localization of precursors of Alzheimer's disease A4 amyloid protein. *Cell.* 57:115–126.

Wilson JR, Williams D, Schachter H. 1976. The control of glycoprotein synthesis: *N*-acetylglucosamine linkage to a mannose residue as a signal for the attachment of L-fucose to the asparagine-linked *N*-acetylglucosamine residue of glycopeptide from α1-acid glycoprotein. *Biochem Biophys Res Commun.* 72:909–916.

Yamashita K, Hitoi A, Kobata A. 1983. Structural determinants of Phaseolus vulgaris erythroagglutinating lectin for oligosaccharides. *J Biol Chem.* 258:14753–14755.

Yazaki M, Tagawa K, Maruyama K, Sorimachi H, Tsuchiya T, Ishiura S, Suzuki K. 1996. Mutation of potential *N*-linked glycosylation sites in the Alzheimer's disease amyloid precursor protein (APP). *Neurosci Lett.* 221:57–60.

Yoshimura M, Ihara Y, Matsuzawa Y, Taniguchi N. 1996. Aberrant glycosylation of E-cadherin enhances cell-cell binding to suppress metastasis. *J Biol Chem.* 271:13811–13815.

Eur J Nucl Med Mol Imaging
DOI 10.1007/s00259-009-1202-1

ORIGINAL ARTICLE

Validation of cardiac ^{123}I-MIBG scintigraphy in patients with Parkinson's disease who were diagnosed with dopamine PET

Kenji Ishibashi · Yuko Saito · Shigeo Murayama · Kazutomi Kanemaru · Keiichi Oda · Kiichi Ishiwata · Hidehiro Mizusawa · Kenji Ishii

Received: 11 March 2009 / Accepted: 9 June 2009

Abstract
Purpose The aim of this study was to evaluate the diagnostic potential of cardiac ^{123}I-labelled metaiodobenzylguanidine (^{123}I-MIBG) scintigraphy in idiopathic Parkinson's disease (PD). The diagnosis was confirmed by positron emission tomography (PET) imaging with ^{11}C-labelled 2β-carbomethoxy-3β-(4-fluorophenyl)-tropane (^{11}C-CFT) and ^{11}C-raclopride (together designated as dopamine PET).
Methods Cardiac ^{123}I-MIBG scintigraphy and dopamine PET were performed for 39 parkinsonian patients. To estimate the cardiac ^{123}I-MIBG uptake, heart to mediastinum (H/M) ratios in early and delayed images were calculated. On the basis of established clinical criteria and our dopamine PET findings, 24 patients were classified into the PD group and 15 into the non-PD (NPD) group.
Results Both early and delayed images showed that the H/M ratios were significantly lower in the PD group than in the NPD group. When the optimal cut-off levels of the H/M ratio were set at 1.95 and 1.60 in the early and delayed images, respectively, by receiver-operating characteristic analysis, the sensitivity of cardiac ^{123}I-MIBG scintigraphy for the diagnosis of PD was 79.2 and 70.8% and the specificity was 93.3 and 93.3% in the early and delayed images, respectively. In the Hoehn and Yahr 1 and 2 PD patients, the sensitivity decreased by 69.2 and 53.8% in the early and delayed images, respectively.
Conclusion In early PD cases, cardiac ^{123}I-MIBG scintigraphy is of limited value in the diagnosis, because of its relatively lower sensitivity. However, because of its high specificity for the overall cases, cardiac ^{123}I-MIBG scintigraphy may assist in the diagnosis of PD in a complementary role with the dopaminergic neuroimaging.

Keywords ^{123}I-MIBG · ^{11}C-CFT · ^{11}C-Raclopride · Scintigraphy · Positron emission tomography · Parkinson's disease

Introduction

Cardiac ^{123}I-labelled metaiodobenzylguanidine (^{123}I-MIBG) scintigraphy has been suggested to be useful for the diagnosis of idiopathic Parkinson's disease (PD), because many recent studies have revealed that cardiac ^{123}I-MIBG uptake decreases with disease progression and that almost all

An Editorial Commentary on this paper is available at http://dx.doi.org/10.1007/s00259-009-1215-9.

K. Ishibashi · H. Mizusawa
Department of Neurology and Neurological Science, Graduate School, Tokyo Medical and Dental University, Tokyo, Japan

K. Ishibashi · K. Oda · K. Ishiwata · K. Ishii (✉)
Positron Medical Center, Tokyo Metropolitan Institute of Gerontology, 1-1 Nakacho, Itabashi-ku, Tokyo 173-0022, Japan
e-mail: ishii@pet.tmig.or.jp

Y. Saito
Department of Pathology, Tokyo Metropolitan Geriatric Hospital, Tokyo, Japan

Y. Saito · S. Murayama
Department of Neuropathology, Tokyo Metropolitan Institute of Gerontology, Tokyo, Japan

K. Kanemaru
Department of Neurology, Tokyo Metropolitan Geriatric Hospital, Tokyo, Japan

Published online: 22 July 2009

patients in the advanced stage of PD show decreased cardiac ^{123}I-MIBG uptake [1–5]. However, it is unclear whether cardiac ^{123}I-MIBG uptake is a good surrogate marker for the diagnosis of PD, especially in early and mild PD cases, which are the most difficult to diagnose in daily clinical practice, because the data on the reduction of cardiac ^{123}I-MIBG uptake in the early stage of PD vary greatly among different studies [1–8]. Therefore, we aimed to investigate the sensitivity and specificity of cardiac ^{123}I-MIBG scintigraphy in diagnosing PD, focusing on early and mild cases of PD in the Hoehn and Yahr (HY) stages 1 and 2.

While planning this study, we focused on dividing the patients into PD and non-PD (NPD) groups in the most appropriate manner in order to acquire precise results. Previous studies have shown that the usual clinical diagnostic accuracy of PD ranges from 70 to 90%, and the accuracy rate greatly decreases in early cases [9–12]. In vivo neurofunctional imaging of the basal ganglia, which provides images of both pre- and postsynaptic nigrostriatal dopaminergic functions, has been recognized as a standard marker for the diagnosis of PD in every clinical stage [13–25]. Therefore, in order to improve the accuracy of the diagnosis of PD, especially in early PD cases, and to classify the patients into the PD and NPD groups in a more appropriate manner, we performed positron emission tomography (PET) imaging with ^{11}C-labelled 2β-carbomethoxy-3β-(4-fluorophenyl)-tropane (^{11}C-CFT) and ^{11}C-raclopride. PET imaging with ^{11}C-CFT and ^{11}C-raclopride can assess the levels of presynaptic dopamine transporter (DAT) and postsynaptic dopamine D_2-like receptor (D_2R), respectively, in the striatum. The two types of PET imaging techniques were together designated as dopamine PET. Further, we proposed the definitions of PD and NPD patterns in dopamine PET findings on the basis of the results which had been confirmed by previous studies.

We also investigated the association between cardiac sympathetic function assessed by cardiac ^{123}I-MIBG uptake, presynaptic nigrostriatal dopaminergic function assessed by striatal ^{11}C-CFT uptake and disease stage determined according to the HY scale.

Materials and methods

Subjects

The present study was a retrospective study. The subjects comprised 39 patients who visited the neurological outpatient clinic at Tokyo Metropolitan Geriatric Hospital from November 2001 to October 2007. They chiefly complained of one or more parkinsonian symptoms, including resting tremor, rigidity, bradykinesia and postural instability. The patients were divided into PD and NPD groups (Fig. 1). Cardiac ^{123}I-MIBG scintigraphy, dopamine PET and magnetic resonance imaging (MRI) were performed for all patients. None of the patients had any concomitant hereditary disorder that could cause parkinsonian symptoms. None of the patients had an individual history of any heart disease. Further, none of the patients were on any medication that could cause parkinsonian symptoms.

For dopamine PET, eight healthy subjects (five men and three women) aged 55–74 years [mean±standard deviation (SD) = 62.3±6.9 years)]were considered as controls. They were deemed healthy based on their medical history, physical and neurological examinations and MRI of the brain. Further, none of them were on medication.

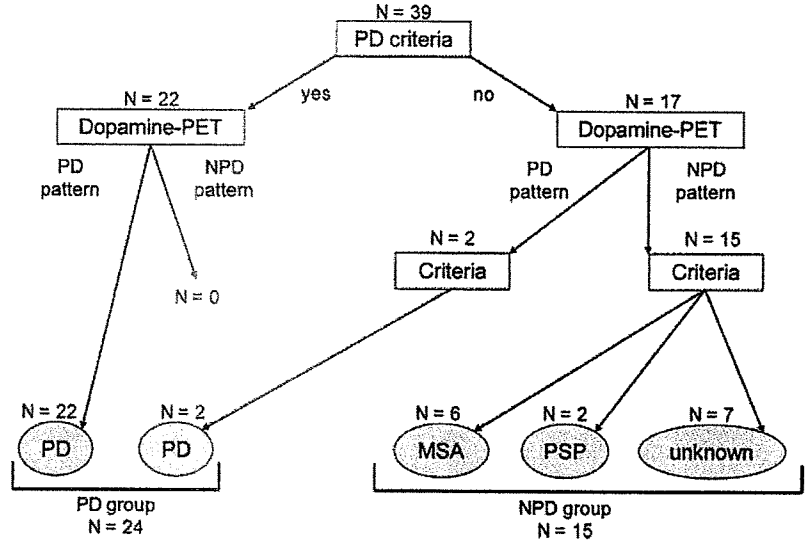

Fig. 1 Diagnostic flow chart and schematic representation of classification process. Patients were classified into PD and NPD groups on the basis of respective published clinical criteria and our dopamine PET findings

This study protocol was approved by the Ethics Committee of the Tokyo Metropolitan Institute of Gerontology. Written informed consent was obtained from all participants.

PET imaging

PET imaging was performed at the Positron Medical Center, Tokyo Metropolitan Institute of Gerontology by using a SET-2400 W scanner (Shimadzu, Kyoto, Japan) in the three-dimensional scanning mode [26], as described previously [27, 28]. The transmission data were acquired using a rotating $^{68}Ga/^{68}Ge$ rod source for attenuation correction. Images of 50 slices were obtained with a resolution of 2×2×3.125 mm voxels and a 128×128 matrix.

Dopamine PET imaging ^{11}C-CFT and ^{11}C-raclopride were prepared as described previously [29, 30]. The two types of PET imaging were performed for all of the subjects on the same day. The patients being treated with antiparkinsonian drugs underwent dopamine PET following at least 15 h deprivation of the medications. Each subject was administered an intravenous bolus injection of 341±62 (mean ± SD) MBq of ^{11}C-CFT, followed by that of 311±56 (mean ± SD) MBq of ^{11}C-raclopride after 2.5–3 h. To measure the uptake of the tracers, static scanning was performed for 75–90 and 40–55 min after the injection of ^{11}C-CFT and ^{11}C-raclopride, respectively. The specific activity of ^{11}C-CFT and ^{11}C-raclopride at the time of injection ranged from 5.9 to 134.2 GBq/μmol and from 10.2 to 201.7 GBq/μmol, respectively.

Analysis of dopamine PET images Image manipulations were performed using Dr. View version R2.0 (AJS, Tokyo, Japan) and SPM2 (Functional Imaging Laboratory, London, UK) implemented in MATLAB version 7.0.1 (The MathWorks, Natick, MA, USA).

The two PET images and one MRI image obtained for each subject were coregistered. The three coregistered images were resliced transaxially, parallel to the anteroposterior intercommissural (AC-PC) line. Circular regions of interest (ROIs) were selected with reference to the brain atlas and individually coregistered MRI images. In each of the three contiguous slices, one ROI with 8-mm diameter was selected on the caudate, two ROIs on the anterior putamen and two on the posterior putamen on both the left and right sides. In other words, the AC-PC plane and regions 3.1 and 6.2 mm above the AC-PC line were selected. A total of 50 ROIs with 10-mm diameter were selected throughout the cerebellar cortex in five contiguous slices.

To evaluate the uptake of ^{11}C-CFT and ^{11}C-raclopride, we calculated the uptake ratio index by the following formula [15, 31]: uptake ratio index = (activity in each region − activity in the cerebellum)/(activity in the cerebellum). We previously validated the method to estimate the binding potential of ^{11}C-raclopride and ^{11}C-CFT, adopting the uptake ratio index [27, 28]. For the further analyses, the uptake of each tracer in each subregion of the striatum (the caudate, anterior putamen and posterior putamen) was evaluated as the average value of the left and right sides. The uptake of each tracer in the whole striatum was evaluated as the average value of entire ROIs in the whole striatum.

Cardiac ^{123}I-MIBG scintigraphy

Scintigraphic studies were performed at Tokyo Metropolitan Geriatric Hospital by using a triple-headed gamma camera (PRISM-3000, Shimadzu, Kyoto, Japan). None of the patients were on any medication, i.e. they were not receiving any drugs such as antidepressants and monoamine oxidase inhibitors, which might influence cardiac ^{123}I-MIBG uptake. After a 30-min resting period, each patient was administered an intravenous bolus injection of 111 MBq of ^{123}I-MIBG (Fujifilm RI Pharma Co., Tokyo, Japan). Planar images of the chest in the anterior view were obtained twice for 5 min, starting at 20 min (early phase) and then at 180 min (delayed phase) after the injection of ^{123}I-MIBG. Relative organ uptake of ^{123}I-MIBG was determined by selecting the ROIs on the heart and mediastinum in the anterior planar image [32]. Average counts per pixel in the heart and mediastinum were used to calculate the heart to mediastinum (H/M) ratio.

MRI

MRI was performed at Tokyo Metropolitan Geriatric Hospital. By using a 1.5-T Signa EXCITE HD scanner (GE, Milwaukee, WI, USA), transaxial T1-weighted images [three-dimensional spoiled gradient-recalled (3D SPGR), repetition time (TR) = 9.2 ms, echo time (TE) = 2.0 ms, matrix size = 256 × 256 × 124, voxel size = 0.94 × 0.94 × 1.3mm] and transaxial T2-weighted images (first spin echo, TR= 3,000 ms, TE=100 ms, matrix size = 256 × 256 × 20, voxel size = 0.7 × 0.7 × 6.5mm) were obtained.

Clinical diagnosis

The diagnostic flow chart is shown in Fig. 1. First, the patients were divided into two groups (22 patients in one group and 17 patients in the other) on the basis of the clinical criteria of the UK Parkinson's Disease Brain Bank (UKPDBB) [10]. Each group was then further classified on the basis of dopamine PET findings. As shown in Fig. 2, the PD pattern in dopamine PET was defined as follows: (1)